Title: Nitrous oxide and methane in Atlantic and Mediterranean waters in the Strait of Gibraltar: air-sea fluxes and inter-basin exchange.

Authors: de la Paz, M[1,2]., I.E.Huertas[1], S. Flecha[1], A.F. Ríos[2] and F.F. Pérez[2].

(1) Instituto de Ciencias Marinas de Andalucía, CSIC, Campus Universitario Río San Pedro s/n, E-11519 Puerto Real, Spain

(2) Instituto de Investigaciones Marinas, CSIC, Eduardo Cabello 6, E-36208 Vigo, Spain

*__Corresponding author:__ Mercedes de la Paz, phone +34 956832612

E-mail: mercedes.delapaz@iim.csic.es

Highlights

- N2O distribution follows the two layers scheme circulation in the Strait of Gibraltar.
- Mediterranean deep waters are highly undersaturated in CH4.
- Nitrification acts as the main N2O source in the Mediterranean overflow water.
- Temperature controls the seasonal variability of N2O in the upper layer.
- The outflow of Mediterranean waters supplies N2O to the North Atlantic.

Abstract:

The global ocean plays an important role in the overall budget of nitrous oxide (N_2O) and methane (CH_4), as both gases are produced within the ocean and released to the atmosphere. However, for large parts of the open and coastal oceans there is little or no spatial data coverage for N_2O and CH_4. Hence, a better assessment of marine emissions estimates is necessary. As a contribution to remedying the scarcity of data on marine regions, N_2O and CH_4 concentrations have been determined in the Strait of Gibraltar at the ocean Fixed Time series (GIFT). During six cruises performed between July 2011 and November 2014 samples were collected at the surface and various depths in the water column, and subsequently measured using Gas Chromatography. From this we were able to quantify the temporal variability of the gas air-sea exchange in the area and examine the vertical distribution of N_2O and CH_4 in Atlantic and Mediterranean waters. Results show that surface Atlantic waters are nearly in equilibrium with the atmosphere whereas deeper Mediterranean waters are oversaturated in N_2O, and a gradient that gradually increases with depth was detected in the water column. Temperature was found to be the main factor responsible for the seasonal variability of N_2O in the surface layer. Furthermore, although CH_4 levels did not reveal any feature clearly associated with the circulation of water masses, vertical distributions showed that higher concentrations are generally observed in the Atlantic layer, and that the deeper Mediterranean waters are considerably undersaturated (by up to 50%). Even though surface waters act as a source of atmospheric N_2O during certain periods, on an annual basis the net N_2O flux in the Strait of Gibraltar is only 0.35±0.27 μmol m^{-2} d^{-1}, meaning that these waters are almost in a neutral status with respect to the atmosphere. Seasonally, the region behaves as a slight sink for atmospheric CH_4 in winter and as a source in spring and fall. Approximating the circulation pattern in the Strait to a bi-layer scheme, N_2O exchange between basins was also calculated, and a net export from the Mediterranean Sea to the Atlantic Ocean equivalent to 39 μmol m^{-2} d^{-1} was found

1. Introduction:

The global ocean contributes markedly to the overall budget of radiatively-active non-CO_2 gases such as nitrous oxide (N_2O) and, to a lesser extent, methane (CH_4); this is because both gases are produced in the marine domain and released to the atmosphere, where they contribute to the greenhouse effect and participate in tropospheric and stratospheric chemical cycling (Crutzen, 1970; 1991). The ocean budgets for N_2O and CH_4 are climate-sensitive, although there are fewer field observations and less understanding of their biogeochemical cycles, in comparison with CO_2 (Garcon et al., 2014). A better assessment of the present oceanic inventories of these greenhouse gases is necessary in order to provide realistic and accurate inputs to predictive models under future climate change scenarios. Improved database is required particularly in the case of N_2O because, according to the IPCC 5th Assessment Report (Ciais et al., 2013), the oceans in total behave as a major natural N_2O source that releases 3.8 Tg-N·year^{-1} to the atmosphere. Similarly, estuaries, rivers and streams emit anthropogenic N_2O, and together release 0.6 Tg-N·year^{-1} (Ciais et al., 2013). These two water sources contribute 20% and 3% respectively to the total global N_2O emissions. Nevertheless, as stated by some authors (Nevison et al., 1995; 2003; Rhee et al., 2009; Bakker et al., 2013), considerable uncertainties arise over these estimates, particularly in coastal areas (upwelling regions, continental shelves, estuaries and mangroves) due to the reduced amount and quality of data currently available. In addition, ocean measurements are also biased to the summer season (Bange et al., 2009), which can lead to an overestimation of the dissolved N_2O concentration when computations are extrapolated to longer timescales. In marine environments N_2O is produced mainly by two microbial pathways: first, as a by-product during nitrification (conversion of ammonia, NH_4^+, into nitrate, NO_3^-) and second, as an intermediate during denitrification (conversion of NO_3^- to dinitrogen, N_2). The presence of the microorganisms that mediate each pathway, and the corresponding N_2O yields, are highly dependent on the concentration of dissolved oxygen (O_2) (e.g., Goreau et al., 1980; Codispoti et al., 2005). Nitrification is one of

98 the processes involved in the aerobic remineralization of organic matter; hence under oxic
99 conditions, as found nearly everywhere in the global ocean, N_2O is formed mainly via
100 nitrification, whereas suboxic to anoxic conditions that favour the net formation of N_2O via
101 denitrification are found only in about 0.1-0.2% of total ocean volume (Codispoti, 2010; Freing et
102 al., 2012).
103 In contrast to N_2O, the contribution of oceanic CH_4 to the global tropospheric CH_4 budget is
104 relatively minor: marine CH_4 emissions represent only a small net input (Ciais et al., 2013).
105 Methane measurements in sediments, where concentrations are in the millimolar scale, were
106 first reported in the mid-1950s, while CH_4 generation in ocean waters was discovered in the late
107 1960s, in part due to measurement constraints as marine CH_4 levels rarely exceed nanomolar
108 levels (Reeburgh, 2007). Since then, even though significant efforts have been made to quantify
109 marine-derived CH_4, the global ocean CH_4 dataset is still quite limited (Bange et al., 2009).
110 Biological production of methane or methanogenesis is the last step in the remineralization of
111 complex organic matter in anaerobic systems and, unlike N_2O, this mechanism requires strictly
112 anaerobic conditions. CH_4 is produced in anoxic sediments, or in the water column via
113 methanogenic bacteria found in sinking particulate matter and in zooplankton fecal pellets (e.g.,
114 De Angelis and Lee, 1994; Karl and Tilbrook, 1994). On the other hand, CH_4 can be consumed
115 via aerobic and anaerobic oxidation occurring in the water column and sediments (e.g. Scranton
116 and Brewer, 1977; Boetius et al., 2000). Nevertheless, although CH_4 concentrations in the open
117 ocean are generally rather low, it has been found that net CH_4 production in the mixed layer
118 leads generally to supersaturation in O_2-saturated near-surface waters, with typical values of
119 130-160%, a phenomenon known as the marine CH_4 paradox (Reeburgh, 2007). The role of
120 phosphate limitation has only recently been discussed as a possible regulator of methane
121 production in oxygenated waters (Karl et al., 2008; Carini et al., 2014). Apparently, under
122 phosphorous limitation, microorganisms increase their consumption of organic phosphorus
123 compounds, such as exogenous methyl phosphonate, that can be converted to methane, as
124 has been demonstrated experimentally (Karl et al., 2008; Carini et al., 2014). Below the ocean
125 mixed layer and away from the oxygen minimum zones, CH_4 concentrations progressively
126 decrease with depth through oxidation, even reaching undetectable levels (Bakker et al., 2013).

Monitoring of both N_2O and CH_4 is then crucial for deciphering the feedbacks between gas formation and emissions, and short- and long-term environmental repercussions.

Currently, these trace gases are measured regularly only at a few time-series sites, such as Station Aloha (Hawaii), CaTS (off Goa, India), Line P (North Pacific), Bocknis Eck (Baltic Sea) and off Chile (Dore et al., 1998; Bange et al., 2010; Naqvi et al., 2010). Assessment of N_2O and CH_4 has recently been incorporated in the regular measurements taken at the Gibraltar Fixed Time series (GIFT) station, located in the Strait of Gibraltar, which connects the Mediterranean Sea and Atlantic Ocean. Data from the GIFT series have been used to estimate biogeochemical fluxes between the two basins (Huertas et al., 2009; de la Paz et al., 2011; Huertas et al., 2012). The exchange of waters masses through the Strait has a strong influence on the general circulation of the Mediterranean and North Atlantic (Peliz et al., 2009); it also regulates the inventories of many chemical compounds in both regions, as is the case of carbon (Álvarez et al., 2005; Flecha et al., 2012), nutrients (Dafner et al., 2003; Bethoux et al., 2005; Huertas et al., 2012), organic matter (Dafner et al., 2001), hydrocarbons (Dachs et al., 1997), trace metals (Van Geen and Boyle, 1990; Elbaz-Poulichet et al., 2001) and radionuclides (Schmidt, 2006; Periáñez, 2008). Therefore, because of its strategic position linking two different marine eco-regions and its role as a sensor for climate change in the Mediterranean (Schroeder et al., 2012), the Strait of Gibraltar represents a node where N_2O and CH_4 monitoring is of particular interest and where no previous measurements have been performed to date. In addition, since complementary biogeochemical and physical parameters are being regularly scrutinized at the GIFT station, our understanding of the processes affecting the distribution of both gases in the region and their transport between the two adjacent basins can be facilitated.

This work provides N_2O and CH_4 data collected for the first time at the surface and in the water column in the Strait of Gibraltar. The aim of our study has been to evaluate the role of this region as a sink or a source of these two gases to the atmosphere by quantifying the air-sea exchange and its temporal variability. Furthermore, the signature of the two trace gases in the inflowing Atlantic and outflowing Mediterranean waters has been analysed, with the N_2O exchange between the two basins also being computed and used to propose a regional balance that considers advected and atmospheric fluxes of this compound. Biogeochemical processes responsible for the spatio-temporal distribution of N_2O and CH_4 in the region are also discussed.

2. Material and Methods

2.1. Study site:

The Strait of Gibraltar is located at the south of the Iberian Peninsula and is the only connection between the Mediterranean Sea and the Atlantic Ocean. It is an east-west orientated channel of a minimum width of 14 km at the Tarifa Narrows (see Figure 1). Circulation in the Strait can be approximated as a bi-layer system formed by the eastward surface Atlantic inflow water (AIW) and the deep westward outflow of saltier Mediterranean Outflow water (MOW), although many physical phenomena occurring at several temporal scales are superimposed over this simple scheme, affecting the magnitude of both flows. The AIW composition is mainly the result of the mixing of the North Atlantic Central Water (NACW, salinity less than 36.06) and a warmer modified form of NACW. For the purposes of this study, the latter will be referred to as Surface Atlantic Water (SAW, salinity about of 36.46) (Gascard and Richez, 1985). Spanish Shelf Water (SSW) and other constituents also influence the composition of the SAW (Van Geen and Boyle, 1990). Similarly, the MOW (salinity 38.2-38.5 and temperature 13-13.5 ºC) is a mixture of Mediterranean intermediate and deep waters, such as the Levantine Intermediate Water (LIW) whose origin is in the eastern basin and which subsequently flows across the Strait of Sicily to join the western Mediterranean and the Western Mediterranean Deep Water (WMDW) formed in the Gulf of Lions. The analysis presented here will focus on the main water masses (SAW, NACW and MOW) comprising the two layers; the remaining constituents of flows are not included explicitly since discrimination between LIW and WMDW requires a very high (almost continuous) sampling frequency, and the contribution of SSW to SAW is minor and intermittent (Bray et al., 1995).

The bottom topography of the Strait is characterized by a main sill on the western side (the Camarinal Sill), which lifts the seabed from a depth of nearly 900 m to a depth of only ~300 m. The interaction between tides and the sharp topography of the channel generate a very complicated hydrodynamic pattern in which undulatory features occur at the Atlantic–Mediterranean Interface (AMI), such as internal bores (Boyce, 1975; Armi and Farmer, 1985),

187 internal waves (Bruno et al., 2002), and horizontal surface divergences. As a result, the
188 Mediterranean outflow entrains the upper Atlantic layer. Therefore, bathymetry, together with
189 meteorological forcing, induces modifications to the two-layer average circulation scheme, with
190 the intensity of the mechanism varying on the tidal to subinertial scale (Garcia-Lafuente et al.,
191 2002).
192 The intense hydrodynamic regime of the Strait has been described as the main forcing agent for
193 the distribution and dynamics of biogeochemical variables in this area. In fact, if hydrodynamic
194 processes were excluded, and only *in situ* biological processes were taken into account, the
195 biogeochemical patterns observed in the AIW could not be explained (e.g., Echevarría et al.,
196 2002; Macías et al., 2008). This local hydrodynamic control over biogeochemistry may even be
197 extended to a larger spatial scale, as has been shown recently in the Western Mediterranean by
198 Naranjo et al. (2014).
199
200 2.2. Methods
201
202 2.2.1. Field sampling and analysis
203 The GIFT time series established in 2005 is formed by 3 stations distributed along the east-west
204 axis of the Strait (Figure 1), where discrete samples are periodically collected at a minimum of 5
205 depth levels. Sampling strategy is aimed at resolving the spatial distribution of biogeochemical
206 variables within the different water bodies that can be differentiated in the Strait and whose
207 positions change both on the vertical scale and longitudinally. Since July 2011, N_2O and CH_4
208 measurements have been added to the set of properties that are routinely studied in the area.
209 This work analyses data collected from that date until November 2014, a period during which 6
210 campaigns were carried out (Table 1). Due to analytical failure, CH_4 results are only available
211 from February 2012. At each station, a temperature and salinity profile was obtained with a
212 SeaBird 911 Plus CTD Probe, which was followed by water sampling with Niskin bottles. Depths
213 were selected on board depending on the position of the AMI at that instant; this position was
214 given by the CTD casts. The uppermost samples were collected at 5 m and the depth of the
215 deepest samples varied with bathymetry, with the deepest level, 860m, being located at Station
216 3. Discrete samples at each level were taken, in this order, for dissolved Oxygen (O_2), N_2O, CH_4

and nitrate. For N_2O and CH_4 two replicates were collected using 120 mL serum vials, sealed with grey-butyl rubber septa and aluminum crimps. Samples were preserved with 250 μL of saturated $HgCl_2$ to inhibit microbial activity. Trace gas samples were stored upside down in the dark, for a maximum of six months, until analysis in the laboratory. Dissolved N_2O and CH_4 were subsequently analyzed by static-headspace equilibration gas chromatography (GC). The analytical equipment is an Agilent 7890 GC with an electron capture detector (ECD) for N_2O and flame ionization detector (FID) for CH_4. The homemade device used for the creation and injection of the headspace in the GC is inspired by the technique developed by Neill et al. (1997) for CO_2 chromatographic analysis, in which 19.7 mL of sample are replaced with a gas of known N_2O and CH_4 composition using a high precision automatic burette (Dosimat 665, Metrohm). The headspace gas is stored in a 5L Tedlar gas-bag before the injection, to ensure that headspace gas is introduced at atmospheric pressure. Following equilibration after a minimum of 12 hours, 18.5 mL of headspace is flushed into the two connected GC sample loops, while introducing a dense brine solution into the bottom of the sample bottle. Then, N_2O and CH_4 are chromatographically separated using two independent Porapak Q packed columns (80-100 mesh; 3 m length for N_2O and 1.5 m for CH_4) operated at 60 ºC and detected with the ECD and FID, respectively. Both separations use ultrahigh purity N_2 as carrier gas (AirLiquide, purity 99.9999%) and, because water vapor and CO_2 interfere in the N_2O analysis, both are eliminated using magnesium perchlorate and Carbosorb® traps located before the packed columns. The system was calibrated using three standard gas mixtures of different origin: a certified NOAA primary standard with composition similar to atmosphere (324.97±0.13 ppb for N_2O and 1863.4±0.3 ppb for CH_4), a second standard gas mixture provided by AirLiquide (France) with certified concentration (1020 ppb for N_2O and 3000 ppb for CH_4) and a secondary standard calibrated against NOAA primary standard (104 ppb for N_2O and 2462 ppb for CH_4) measured routinely every 4 samples to check the GC stability. The precision of the method estimated from the coefficient of variation based on replicate analysis of water samples (n=10) was 0.6% for CH_4 and 0.4% for N_2O. The equilibrated mixing ratios corrected for phase partitioning during analysis were computed following Upstill-Goddard et al. (1996). Dissolved concentrations were determined by applying the expressions for solubility proposed by Weiss and Price (1980) and Weisenburg and Guinasso (1979) for N_2O and CH_4, respectively.

O_2 samples were taken in a sealed glass flask and stored in darkness for 24 h, as described by the Winkler method, for later analysis by potentiometric titration (Metrohm 794 Titroprocessor), with an estimated uncertainty of ±1µmol kg^{-1}.

For nitrate, three replicates of 12 mL of filtered seawater (Whatman GF/F filters) were taken from the Niskin bottle and stored at -20ºC. Concentration of nitrate was measured in the laboratory using a TRAACS800 (Bran+Luebbe) auto-analyzer and the techniques of Grasshoff et al. (1983). The standard deviation for the mean of all replicates was 0.06 µmol kg^{-1} for nitrate.

2.2.2. Calculations

The saturation values of O_2 were calculated with the equation given by Benson and Krause (UNESCO, 1986) and the Apparent Oxygen Utilization (AOU) was defined as the difference between the oxygen concentration at saturation and the observed oxygen concentration.

Apparent N_2O production was calculated as the difference between the observed N_2O concentration and the expected N_2O concentration in the equilibrium at the corresponding temperature (Yoshinari, 1976), in a similar way to the AOU concept, hence:

$$\Delta N_2O = [N_2O]_{observed} - [N_2O]_{equil} \quad \text{Eq. (1)}$$

Saturation values expressed as percentage (%) for N_2O and CH_4 were computed as the ratio between the gas concentration measured and the calculated equilibrium concentration for N_2O and CH_4. On the one hand, the calculations of the equilibrium concentrations in the entire water column (deeper than 25 m) were done using the mean global atmospheric ratios for the study period (2011-2014) in order to obtain a homogeneous long-term vertical signal for the N_2O and CH_4 saturation values. These atmospheric mixing ratios for N_2O (xN_2O_{atm}) and CH_4 (xCH_{4atm}) were provided by the World Data Center for Greenhouse Gases (http://ds.data.jma.go.jp/gmd/wdcgg/). Such mean values were calculated as 325 ppb and 1818 ppb for xN_2O_{atm} and xCH_{4atm} respectively. On the other hand, the surface layer is affected by a short-term exchange with the overlaying atmosphere, therefore the saturation values in the upper 25 m layer, and air-sea flux computation of both gases, were computed using monthly mean measurements from the two meteorological stations nearest in latitude to the Strait of Gibraltar, namely Mace Head (Ireland, 53.33 ºN) and Izaña (Tenerife, Spain, 28.3 ºN) (http://ds.data.jma.go.jp/gmd/wdcgg/). Due to the marked latitudinal gradient of CH_4, and to a

277 lesser extent for N_2O (Dlugokencky et al., 1994), atmospheric ratios from these two
278 meteorological stations were linearly interpolated versus latitude. For consistency,
279 measurements data from the NOAA/ESRL were used in both cases, xN_2O_{atm} and xCH_{4atm}, and
280 the values are summarized in Table 2.
281 The gas air–sea flux (F) was calculated as:
282 $F = k_w (C_w - C_a)$ Eq. (2)
283 where k_w (cm h^{-1}) is the gas transfer coefficient as a function of wind speed at 10 m height (U_{10}
284 in m s^{-1}), C_w is the measured N_2O seawater concentration, and C_a is the equilibrium N_2O
285 concentration in seawater based on the molar atmospheric ratio explained above. k_w was
286 calculated based on the combined linear and quadratic k_w–*wind speed* relationship proposed by
287 Nightingale et al.(2000): $k_w = 0.222\ U_{10}^2 + 0.333\ U_{10} * (Sc/600)^{-1/2}$ Eq. (3)
288 where Sc is the Schmidt number calculated for N_2O and CH_4 as a function of the temperature,
289 according to Wanninkhof et al. (1992). The wind speed data were provided by Puertos del
290 Estado, recorded at the buoy moored in the Gulf of Cadiz, and then corrected to 10 m height
291 using the formula by Large and Pond (1981). Daily averaged wind speed was used for the k_w
292 calculation.
293
294 2.2.3. Water transport and N_2O exchange through the Strait of Gibraltar
295 Computation of the flux of N_2O through the Strait requires a proper identification of the two
296 layers that form the inverse-estuarine exchange of waters in the Strait. Previous studies have
297 reported that this bi-layer scheme results in a mean net transport $Q_0 = Q_{AIW} + Q_{MOW}$, equal to
298 0.038 ±0.007 Sv (Sverdrups, 1 Sv=10^6 m^3 s^{-1}) [Soto-Navarro et al., 2010], which is equivalent to
299 a net evaporation of 0.6 m y^{-1} in the Mediterranean, and where Q_{AIW} and Q_{MOW} stand for the
300 transport of Atlantic and Mediterranean waters respectively. In this work, the continuous
301 measurements of Q_{MOW} recorded at the Espartell Sill (Figure 1) and provided by Huertas et al.
302 (2012) have been used. Details regarding equipment, data recording and treatment are
303 explained in Sánchez-Román et al. (2009). From Q_{MOW} and taking into account the long-term
304 barotropic flow (Q_0), computation of Q_{AIW} is straightforward. Since the depth and thickness of
305 the interface between the two water masses are highly variable throughout the channel due to
306 topography and hydrodynamic processes occurring at different temporal scales, the interface

307 that marks the separation of layers has been identified here according to the salinity criterion
308 given by Huertas et al. (2012). Briefly, at the westernmost part of the Strait (ES, St 1), a salinity
309 of 37.0 delimits the boundary between AIW and MOW and consequently, the portion of the
310 water column exhibiting lower salinity values than those chosen for AMI definition was
311 incorporated into the AIW, whereas the rest of the water column down to the sea floor was
312 included within the MOW. From this it was possible to calculate a mean N_2O concentration in
313 each layer, which was required for the calculation of the net flux of this gas through the Strait
314 according to the equation:
315
316 $$F_N = F_{MOW} - F_{AIW} = (\rho_{MOW} \times Q_{MOW} \times [N_2O]_{MOW}) - (\rho_{AIW} \times Q_{AIW} \times [N_2O]_{AIW}) \quad \text{Eq. (4)}$$
317 where ρ, Q and $[N_2O]$ indicate water density, water transport and mean N_2O concentration in
318 each layer; and so F_{MOW} and F_{AIW} denote the N_2O fluxes into the Mediterranean and the Atlantic
319 respectively. Densities for the MOW and AIW were 1029 and 1027 kg m^{-3}, respectively.
320
321 **3. Results and discussion**
322
323 **3.1. East-West and vertical distribution of N_2O and CH_4**
324 Figure 2 shows the spatial distribution of N_2O and CH_4 in the Strait of Gibraltar together with the
325 thermohaline properties in the water column, O_2 and nitrate, for the cruise performed in May
326 2013 as a snapshot. The most remarkable feature for all the properties is the pronounced
327 vertical gradient, which can be linked to the presence of the AMI delimited by isohaline 37 at the
328 westernmost station. The interface can be traced by a sharply halocline (Fig. 2), extending from
329 east to west throughout the whole channel. As previously described (e.g., Bray et al., 1995;
330 Huertas et al., 2009), the location of the AMI becomes more shallow toward the east, moving
331 from 150 m depth at the western station to 60 m at station 3; the AMI is therefore deeper,
332 thicker, fresher and colder in the westernmost part of the Strait. The upper layer mainly
333 corresponds to the SAW, with typical salinity around 36.4 and a surface temperature of 18 ºC
334 on the western side and 17 ºC on the eastern side for this particular time of the year (Fig. 2 and
335 Fig. 3). Below the AMI, the deeper layer filled by the MOW occupies a larger volume in the
336 water column on the eastern side and its presence is characterized by temperatures ranging

337 from 13.0 to 13.4 ºC and salinity above 38.00 (Fig. 2). Dissolved O_2 decreases with depth and
338 concentrations fluctuate from 243 µmol kg^{-1} on the surface (St1) (SAW) to a minimum of 162
339 µmol kg^{-1} at 250 m depth on the eastern side of the channel, coinciding with the presence of the
340 "Mediterranean tongue" (Fig. 2). The O_2 distribution observed here follows the east-west and
341 vertical features already reported by other studies, with concentrations also being in line with
342 those measured in the past (Minas et al 1991; de la Paz et al 2008). Nitrate concentration
343 shows minimum values (undetectable levels < 0.06 µmol kg^{-1}) within the upper 50 m of the
344 water column in the westernmost part of the Strait, and increases to a maximum of 10.2 µmol
345 kg^{-1} within the MOW (St3, 250 m depth) coinciding with the O_2 minimum. East of the Camarinal
346 Sill, nitrate levels in the upper layer increase and reach 3.6 µmol kg^{-1} (Fig. 2). This nutrient
347 enrichment may be attributable to mixing processes occurring from the interaction of the two
348 main flows at this particular section of the Strait, where the nutrient-enriched MOW injects
349 nitrate into the AIW (Macías et al., 2007a). The spatial distribution of nitrate and the levels
350 observed here are in agreement with those measured in the past (Minas et al., 1991; Dafner et
351 al., 2003; de la Paz et al., 2008; Macías et al., 2007a) and with more recent observations at the
352 GIFT time series station (Huertas et al., 2012).
353 The spatial pattern for N_2O distribution follows closely those for O_2 and nitrate (Fig. 2). Thus,
354 N_2O concentration presents minimum values at the surface layer of the western entrance of the
355 Strait, increasing gradually towards the east; in May 2013, this increasing latitudinal gradient
356 varies from 7.79 nmol kg^{-1} at St. 1 to 8.94 nmol kg^{-1} at St. 3. In addition, N_2O increases with
357 depth, to 11.25 nmol kg^{-1} in the MOW, coinciding with the minimum in O_2 concentration. Unlike
358 the rest of the properties analysed, CH_4 did not show a clear vertical distribution associated with
359 the bi-layer circulation scheme (Fig. 2) although it still shows a trend in which higher
360 concentrations are present in the upper layer and diminish with depth to a minimum.
361 When the bulk of the data collected in all the campaigns is considered, a vertical gradient for
362 temperature, salinity, N_2O and CH_4 is also clearly noticeable (Fig. 3). Temporal variability of
363 these parameters can be seen particularly in the upper layer (see Fig. 3), where θ, N_2O and CH_4
364 concentrations show the most variability; this may be related to the temperature cycle on the
365 seasonal scale, as analyzed in detail in section 3.4. Regarding the water column at lower
366 depths, the high vertical variability observed between data obtained on different cruises and at

depths between 50 and 300 m may be attributed both to the position of the AMI during sampling and to tidally-induced hydrodynamic processes.

The general trends described for the cruise performed in May 2013 (Fig. 2) reflect the vertical trends when the complete database is evaluated (Fig. 3): thus, in the upper 25 m, salinity and temperature values range from 35.8 to 36.6 and from 14.7 to 23.44 ºC respectively, corresponding to the thermohaline properties of the SAW. Then temperature progressively decreases as salinity increases moving through the AMI; below the interface, temperature and salinity show low spatio-temporal variability compared to the upper layer, with values varying from 12.9 and 13.4 ºC and from 38.0 to 38.5 respectively. N_2O concentrations in the upper layer oscillate from 6.55 to 8.83 nmol kg^{-1} and increase progressively with depth following the distribution of the two main water masses (AIW and MOW); and below 300 m depth, where only MOW is found, N_2O concentrations range from 9.68 to 11.25 nmol kg^{-1}. CH_4 concentrations show the opposite trend to N_2O: data collected in February 2012 and May 2013 fall within a similar range of concentrations in the upper layer (for salinity < 37.0; 1.56–2.78 nmol kg^{-1}) and minimum CH_4 concentrations were observed at depths below 300 m at Station 3, with values ranging from 1.13 to 2.0 nmol kg^{-1}. On the other hand, CH_4 measurements in November 2014 present maximum levels around 150 m extending from West to East, and unexpectedly reach the highest values recorded, equivalent to 4.94 nmol kg^{-1} at Station 1, which subsequently decrease eastwards (Fig. 3). This vertical pattern corresponds to an episodic event, since that cruise was performed immediately following an intense storm that lasted nearly 3 weeks with high winds of 20 m s^{-1}, which may have pushed coastal waters with elevated levels of CH_4 (Ferrón et al., 2010a) towards the Strait or may have resuspended sediments that also contributed to increased CH_4 concentrations.

3.2. N_2O and CH_4 distribution within water masses

Identification of water masses present in the Strait can be also derived from the T-S plot shown at the top of Figure 4; this plot brings together the complete set of data collected at the GIFT station during the six cruises conducted. Fig. 4a reveals the presence of three main water masses: the SAW, which is detected on the upper left side, with salinity nearly constant (~36.4) and a temperature fluctuation of ~ 6ºC as a result of the seasonal variations. The salinity

minimum detected in the lower left corner of Fig. 4a corresponds to the footprint of the NACW, with a more frequent presence on the westernmost side of the Strait at a depth of around 100 m, in agreement with previous observations at the GIFT station (Huertas et al., 2009). The MOW can be identified in the right lower corner of the T-S plot, with a very constant signature during all the cruises along the longitudinal axis of the Strait. The AMI is also distinguishable in the lower part, being characterized by a salinity gradient, since it is the result of mixing between two water bodies, the AIW and the MOW. This description matches the classic T-S pattern described traditionally in the region (Gascard and Richez, 1985). Regarding the presence of each water mass, Bray et al. (1995), using temperature and salinity data of 313 vertical CTD profiles obtained at different times of the year, estimated that, on average, the composition of the upper layer is 50% SAW, 40% NACW and 10% MOW, whereas in the lower layer, the composition is 90% MOW, 2% SAW and 8% NACW. More recent studies based on continuous recordings indicate that the presence of NACW in the lower layer is almost zero (García-Lafuente et al., 2007).

Biogeochemical differences between the NACW and the SAW can be identified from the AOU-salinity pattern (Fig. 4b). In particular, it is evident that AOU values of up to 60 μmol kg^{-1} may be associated with salinities close to 36.0; these values decrease progressively with salinity, and fall to almost 0, even reaching negative values at salinities lower than 36.5. These AOU signals coincide with those observed in earlier studies conducted in the Strait and in the nearby Gulf of Cadiz (Ait-Ameur et al., 2006; Flecha et al., 2012), which distinguished the presence of two types of NACW: the warmer Eastern North Atlantic Central Water of subtropical origin, which is oxygen-saturated, and the colder subpolar Eastern North Atlantic Central Water, located below the former in depth, in which the AOU levels increase (Ríos et al., 1992; Pollard et al., 1996; Pérez et al., 2001). Pérez et al. (2001) attributed the deeper AOU maximum to the remineralization of organic matter near the coast of Africa linked to the northwest African upwelling system.

In the various different water masses, the relationship between N_2O and salinity (Fig. 4c) closely resembles the AOU pattern The maximum N_2O concentration in the Atlantic inflow of around 10.6 nmol kg^{-1} (cruise July 2011, St. 1, depth 175 m) was found at the salinity value of ~36.0 that marks the presence of the NACW, with levels decreasing down to 6.5 nmol kg^{-1} at salinity

427 36.5 (cruise July 2011, St. 1, depth 10 m), which is indicative of the SAW. As for AOU, the N_2O
428 distribution suggests that the N_2O signature differs between the two branches of the AIW, with a
429 higher N_2O content being present in the NACW compared with the SAW (Fig. 4.c). The highest
430 N_2O concentrations observed in the Strait (between 9.68 and 11.25 nmol kg^{-1}) are present in the
431 MOW, as they were measured at salinities > 38 (Fig. 4.c). Both NACW and MOW were
432 oversaturated in N_2O, with oversaturation values up to 120 % and 124%, respectively. AOU and
433 N_2O show a similar relationship with salinity, with a nearly straight line of mixing between the
434 Atlantic water masses (SAW and NACW) and the MOW, suggesting that both variables are
435 acting as conservative parameters; this behavior is not surprising in the Strait of Gibraltar, as it
436 was previously described for O_2 (Minas et al., 1991), because the time scales of mixing
437 processes are too short to allow changes through biological activity. In contrast, CH_4 levels did
438 not show a clear relationship with salinity (Fig. 4.d), although higher CH_4 concentrations (up to
439 4.94 nmol kg^{-1} in Nov 2014) were generally observed in the shallower SAW, and the lower
440 values could be associated with the MOW (1.13 nmol kg^{-1}). In the surface layer CH_4 oscillates
441 between undersaturation in February 2012 (88%) and oversaturation in November (133%), with
442 the saturation level decreasing to 47% in the MOW.
443 No direct observations for N_2O or CH_4 in the Strait of Gibraltar have been found in the literature.
444 Ferrón et al. (2010a; b) described the spatiotemporal variability of the two gases in coastal
445 waters of the adjacent north-eastern shelf of the Gulf of Cadiz. That study reported a steep
446 gradient of both N_2O and CH_4 from the continent to the ocean, as the inner zone of the shelf is
447 strongly affected by river and continental inputs; its authors reported values for CH_4 in May
448 2007 that reached concentrations as high as 28.61 nM in bottom waters, whereas a minimum of
449 1.64 nM was measured in surface offshore waters, corresponding to saturation values of 108%
450 and 100% respectively (Ferrón et al., 2010a). In the case of N_2O, levels varied from 8.2 nM in
451 May 2007 to 28.5 nM in November 2006, which correspond to saturation values of 100% to
452 335%, respectively, for the region of the Gulf closer to the Strait of Gibraltar, with less influence
453 of continental inputs (Ferrón et al., 2010b). Our study shows concentrations of N_2O in the Strait
454 that are more similar to those found by Walter et al. (2006) in oceanic waters of the cold-
455 temperate North Atlantic. In fact, these authors reported relatively uniform N_2O concentrations
456 of around 8.5 nmol kg^{-1} in the surface layer, and higher values (~11.3 nmol kg^{-1}) below the

457 thermocline and down to the bottom. Moreover, Forster et al. (2009) also gave ranges of N_2O
458 and CH_4 in the North Atlantic that roughly match the values observed for both the NACW and
459 SAW in the Strait of Gibraltar. The low CH_4 values found in the MOW (Fig. 2f and 4d) are similar
460 to the CH_4 levels in deep waters reported in other studies, such as those of Keir et al. (2005) in
461 the Northeast Atlantic and Yoshida et al. (2011) in the South Pacific.
462
463 **3.3. Biogeochemical processes and N_2O and CH_4 patterns in the Strait of Gibraltar**
464 The most relevant biogeochemical parameters analyzed in relation to N_2O distribution are those
465 assumed to be directly connected with the production pathways of this gas, such as oxygen,
466 AOU and nitrate (NO_3^-). In our study, positive relationships are found between ΔN_2O and AOU
467 (Fig. 5.a; r^2=0.73) and between ΔN_2O and NO_3^- (Fig. 5.b; r^2=0.62) for the complete database,
468 which indicate that nitrification is indeed favored when oxygen concentration decays in the
469 medium and would be consistent with the proposition that nitrification is the major production
470 process in the North Atlantic (Yoshinari, 1976; Oudot et al., 2002; Nevison et al., 2003).
471 Typically, the slope of the correlation between ΔN_2O and AOU provides a means to estimate the
472 N_2O yield per O_2 molecule consumed during nitrification. Therefore, the slope of the regression
473 line of ΔN_2O vs AOU gives a rough estimate of N_2O production per mole of O_2 consumed; in the
474 Strait of Gibraltar this approach gives a result of 0.018 nmol N_2O/µmol O_2. However, in the
475 particular case of the Strait of Gibraltar, where the water column is characterized by intense
476 advection in the AIW and MOW layers, and by a marked vertical mixing, the slope of the
477 correlation between ΔN_2O and AOU can also reflect phenomena superimposed over the
478 nitrification process, particularly in the upper layer; this could therefore lead to a
479 misinterpretation of the trend. As shown in Fig. 5, a different range of variability for ΔN_2O and
480 AOU can be detected in the AIW compared to that in the MOW. In fact, taking into consideration
481 the plots of AOU and N_2O versus salinity (Fig. 4), which depict a conservative behavior during
482 mixing in the AMI, it may be that the high degree of correlation between ΔN_2O and AOU is also
483 the result of the conservative pattern of the two properties during mixing of the AIW and MOW
484 at the interface layer.
485 Nevison et al. (2003) evaluated the global distribution of the ΔN_2O-AOU yield in the subsurface
486 ocean and found that correlation slopes between ΔN_2O and AOU are not a reliable gauge of the

biological N_2O yield per mole of O_2 consumed, because the slopes are strongly influenced by mixing gradients. They also concluded that the ΔN_2O/AOU ratio calculated from individual data pairs, rather than from the ΔN_2O- AOU correlation, offers the best means of estimating the biological yield of N_2O production per mole of O_2 consumed. Therefore, the ΔN_2O/AOU ratio from each pair of data has been computed in this study. As a result, the ratios in figure 5 show very scattered values for AOU levels, less than 40 μmol kg^{-1}, that are consistent with the SAW values and with the N_2O values that are also near saturation (see Fig. 4), whereas for AOU levels higher than 40 μmol kg^{-1}, corresponding, in the AOU-salinity diagram (Fig. 4), to the NACW and the MOW, the ΔN_2O/AOU ratios range between 0.013 and 0.032 nmol N_2O/μmol O_2. The average ratio calculated for the NACW (AOU> 40; salinity<36.5) is 0.029±0.005 nmol N_2O/μmol O_2, and 0.020±0.003 nmol N_2O/μmol O_2 in the case of the MOW (AOU>60; salinity>38). ΔN_2O/AOU ratios in the Strait are relatively low compared to other ocean regions although, despite the slight fluctuations observed, our estimations fall within the range of those previously found by Walter et al. (2006) in the North Atlantic, with slope values between 0.022 and 0.045 for cold temperate latitudes, which are also consistent with the values given by Nevison et al. (2003); the latter authors pointed out that the lowest values of the ΔN_2O/AOU ratio are found in the Atlantic Ocean and are equivalent to 0.02 at latitudes between 20 and 40 ºN. Unfortunately, there are no previous estimations of the ΔN_2O/AOU ratio in the MOW passing through the Strait, or in the Mediterranean basin, that would enable a specific comparison to be made with the values obtained in our study. In fact, the N_2O concentrations presented here are the first measurements made in the MOW, and so may serve as a starting point for tracking the evolution of this trace gas in the Mediterranean Sea by means of continuous monitoring of the MOW at the GIFT time series station. Recently, current values of nitrate and AOU have been reported on a basin scale in a wide study carried out by Tanhua et al. (2013). The distribution of this parameter can be used as an approach to evaluate nitrification processes in the Mediterranean, as these authors compiled biogeochemical data collected in 2011 during 3 oceanographic cruises covering an east-west section from the Gulf of Cadiz to the Levantine Basin (Tanhua et al., 2013). According to these latter results, the Mediterranean Sea is well oxygenated, and even the oxygen minimum layer (OML) found at intermediate depths is characterized by oxygen concentrations of the order of 180 μmol kg^{-1} (AOU~70-80 μmol kg^{-1}).

517 This finding may be attributed to the active and rapid ventilation of the Mediterranean Sea
518 (Roether and Schlitzer, 1991; Stöven, 2011), and to the low rate of primary production present
519 in the surface waters of certain Mediterranean sub-basins (Pujo-Pay et al., 2011). The relatively
520 low AOU values found in the Mediterranean Sea support the low ΔN_2O/AOU ratio observed in
521 the Strait in relation to those characterizing other ocean regions. Even though the ΔN_2O/AOU
522 ratio is low, nitrate and AOU concentrations within the MOW (Fig. 4) coincide with the maximum
523 levels of both parameters found at deep and intermediate waters in the Western basin by
524 Tanhua et al. (2013). N_2O production is particularly relevant in several "hot spot" regions, such
525 as the eastern tropical Pacific and the Arabian Sea, where O_2 falls to very low levels and the
526 ΔN_2O/AOU ratio is one order of magnitude higher than that reported in this study (up to 0.27
527 nmol N_2O/μmol O_2). Apart from these areas, there is a less intense but significant production
528 whose distribution varies with O_2 and depth (Nevison et al., 2003).
529 Unlike N_2O, CH_4 did not exhibit any significant correlation with AOU, nitrate or any other
530 biogeochemical parameter in the Strait. Generally in the ocean, surface waters are
531 oversaturated in CH_4, and sometimes maxima also occur at the base of the thermocline,
532 associated with the chlorophyll maximum. This common feature is not discernible in the Strait of
533 Gibraltar, which is probably due to the reduced chlorophyll and primary production present in
534 this region due to the low residence time of the waters moving along the Strait (Minas et al.,
535 1991; Macías et al., 2007a). The average CH_4 saturation in the SAW and NACW
536 (salinities<36.5; z>25 m depth) is 74±16%, whereas the most striking feature is that the vertical
537 profile of CH_4 depicts high undersaturation values within the MOW, with average
538 undersaturation equal to 66±16% (salinity>38). This finding can be attributed to the oxidative
539 consumption of methane during the transit time of this water mass passing through the
540 Mediterranean basin; clearly more data would be required to discern any vertical trend or
541 identify the processes underlying such variability. Furthermore, CH_4 measurements in
542 November 2014 show maximum concentrations at a depth of around 150 m extending from
543 West to East and reach unexpectedly the highest values recorded (Fig. 3), equivalent to 270%,
544 in the AIW layer, which subsequently decrease eastwards; but surprisingly, the CH_4 saturation
545 values at the surface and in the deep layer show similar values in other cruises (Fig. 3). As
546 already mentioned, this vertical pattern corresponds to an episodic event, since that cruise was

made immediately following an intense storm that lasted nearly 3 weeks. There are several possible explanations for this CH_4 source: advection from coastal water from the Gulf of Cadiz with elevated levels of CH_4 (Ferrón et al., 2010a) towards the Strait, remobilization of sediments that also contributed to increased CH_4 concentrations; and storm-induced methane release from the mud volcanoes or diapiric structures hosting methane-hydrate that are abundant in the continental margin of the Gulf of Cadiz (Somoza et al., 2002). Although some studies indicate that CH_4 originated in those mud volcanoes from the Gulf of Cadiz is completely consumed due to the intense microbial consumption on the seafloor (Niemann et al., 2006), the impact of the episodic storm could have induced the release of CH_4, as previously reported in other continental margins, such as in the Arctic continental shelf (Shakhova et al., 2007).

3.4. N_2O and CH_4 in the surface layer: seasonality of gas distribution and the air-sea exchange

The surface water properties in the Strait of Gibraltar are those corresponding to the SAW, which is the main contributor to the upper AIW, since the NACW appears normally at intermediate depths at the westernmost part of the Strait (Stations 1 and 2; 100-150 m depth; Fig. 2, Fig. 3). Further, the minimum surface seawater temperature (SST) recorded for our study period was 15 ºC in February 2012, whereas a maximum SST of 22 ºC was recorded in July 2011. In order to evaluate the seasonal coverage of our dataset, the surface SST in the Strait of Gibraltar was compared with the continuous temperature record for our study period (2011-2014) obtained at a buoy moored in the Gulf of Cadiz that is part of the marine observational network of Puertos del Estado. Fig. 6 shows the climatological mean of SST calculated from the buoy data. The high correlation found between our discrete temperature measurements and the continuous records confirms that our dataset covers appropriately the minimum, maximum and inflection points of the sinusoidal shape of the seasonal variability, and hence, possesses a good seasonal coverage and is representative of the annual temperature cycle. In comparison to the seasonal variability of SST, salinity variations in the SAW were very small (see Fig.3) and ranged from 35.95 to 36.5.

In order to identify and evaluate the seasonal cycle of N_2O and CH_4 concentrations in surface waters, averaged data for each cruise in the upper 12 m (the sampling depth closest to surface

577 repeated most frequently during all cruises, see Fig.3) were considered. The N_2O surface
578 concentration showed the maximum values (8.74±0.13 nmol kg^{-1}) in February (Fig. 6),
579 coinciding with the minimum annual temperature, whereas the lowest N_2O surface
580 concentration was measured in July (7.19±1.06), when the maximum temperature for our study
581 period was recorded. The surface layer was nearly in equilibrium with the atmosphere, with
582 saturation values of 100 %, during the cruises carried out in winter and spring, and slightly
583 oversaturated during summer (Table 2). These results suggest that temperature is the main
584 factor responsible for the seasonal variability of N_2O in the surface layer. The amplitude of the
585 annual range of salinity recorded in the Strait (0.5 salinity units) had only a minor impact on the
586 solubility variations at the surface (1%). The annual influence of temperature on gas
587 concentration (Table 2) can be evaluated from the ratio between the seasonal amplitude of the
588 N_2O observed (=1.6 nmol kg^{-1}) and the seasonal amplitude of N_2O saturation concentration
589 (=1.8 nmol kg^{-1}). Accordingly, temperature variations would explain 87% of the seasonal
590 variability of N_2O at the surface layer, suggesting that N_2O surface concentration is driven
591 mainly by solubility. Freing et al. (2009) demonstrated that both N_2O surface concentration and
592 air-sea N_2O fluxes in the North Atlantic follow a seasonal cycle similar to that of CO_2. This
593 seasonal cycle can be described by a harmonic function and is controlled primarily by
594 temperature, allowing the computation of a reasonably accurate mean flux. In this area, de la
595 Paz et al. (2011) demonstrated, by reconstructing the CO_2 seasonal cycle with data collected
596 during 36 cruises, that solubility is also the main mechanism governing CO_2 concentration in
597 surface waters. In contrast to the trend found in the Strait of Gibraltar, a positive correlation
598 between temperature and N_2O oversaturation was also found in the nearby coastal waters of
599 the Gulf of Cadiz, which was attributed to the enhancement of nitrification during the summer
600 time due to the increasing bacterial activity with temperature, as this area is considerably
601 affected by organic matter inputs from estuaries and aquaculture activities (Ferrón et al.,
602 2010b).
603 Regarding the contribution of other factors, such as biological processes, to gas distribution in
604 surface waters of the Strait, it is worth pointing out that *in situ* observations and modelling
605 studies have reported a very fast transit time of particles due to the strong advection, especially
606 in the upper layer, and hence significant phytoplankton growth cannot be sustained (Macías et

607 al., 2007a). The upper layer in the central channel of the Strait that flows rapidly towards the
608 Mediterranean is normally considered oligotrophic. In theory, primary productivity usually leads
609 to the generation of organic matter, which, being subsequently recycled, may be a potential
610 source of N_2O. This is not clearly the case in the Strait, as surface oligotrophy, together with the
611 high oxygen availability, would result in a low or insignificant nitrification activity.
612 In order to examine short-term variability of N_2O and other possible sources of variability in the
613 upper layer, we evaluated the deviations of the measured N_2O concentrations with respect to
614 the average cruise values for N_2O, hereinafter named the "N_2O anomaly". Similarly, the SST
615 anomaly has been computed as the difference between each value of SST measured
616 individually and the averaged SST of the cruises. Figure 7 shows the high negative correlation
617 found between the SST anomaly and the N_2O anomaly (r^2=0.81). Positive anomalies
618 correspond to St. 1, whereas negative anomalies are mainly observed in St. 3. However, those
619 anomalies show no seasonal pattern or correlation with SST or salinity. This is consistent with
620 the hypothesis that N_2O-enriched colder water could be brought to the surface via vertical
621 mixing. The distribution pattern of SST, nitrate and other parameters in surface water exhibit a
622 marked east-west variability, which can be attributed to the presence of internal waves, as has
623 previously been described for dissolved inorganic carbon (de la Paz et al., 2008) and for CO_2
624 (de la Paz et al., 2011). These internal waves generated at the Camarinal sill lift the interface
625 and trigger the upwelling of N_2O-enriched deeper waters that then enter the upper surface layer.
626 In addition, the bathymetry of the channel causes the AMI to uplift towards the east, being
627 shallower at St. 3, where the MOW occupies a larger volume of the water column. The detection
628 of water-ascending events triggered by internal waves based solely on salinity changes is,
629 however, difficult. Other sources of variability in N_2O content have been explored, such as wind
630 speed, but no correlation was found. Contrary to the waters proximal to the Strait, where a clear
631 relationship between zonal winds and upwelling episodes has been identified, both in the Gulf of
632 Cadiz (Navarro et al., 2006) and in the Alboran Sea (Macías et al., 2007b), these wind-induced
633 upwellings are not expected to be relevant in the channel, due mainly to the one-dimensional
634 character of the flow in the Strait of Gibraltar, which is characterized by very high current
635 velocities.
636

637 As for CH_4, Figure 6 depicts the minimum concentration in the surface waters observed in
638 February 2011 (2.16±0.14 nmol kg^{-1}) and the maximum level in November 2014 (2.79±0.22
639 nmol kg^{-1}). Accordingly, saturation at the surface layer varied between 93% in February 2012
640 and 126% in November 2014. Oversaturation in November and May is in agreement with typical
641 saturation values of CH_4 in oceanic waters, which are of the order of 120% (Reeburgh, 2007).
642 However, there is no obvious explanation for the slight undersaturation reported in February
643 since no correlation was found between CH_4 and SST or salinity and thus further
644 measurements are required for a more comprehensive analysis. It is noteworthy that similar
645 CH_4 undersaturation values (~ 95%) were also reported for February in 2007 in the offshore
646 waters of the Gulf of Cadiz by Ferrón et al.(2010a). On the other hand, there was no evidence
647 for *in situ* production during May or November that could account for the oversaturation values,
648 since no consistent correlation was observed between CH_4 concentrations and biogeochemical
649 parameters such as chlorophyll or nutrients data that are available in the GIFT database.
650 Unfortunately, there are insufficient data on CH_4 in surface water to allow the proper
651 identification of the seasonal cycle. The saturation anomaly (ΔCH_4) has been signaled as the
652 major factor of uncertainty in the determination of the CH_4 air-sea fluxes in oceanic waters
653 (Rhee et al., 2009) due to limitations in the instrumental determination of ΔCH_4, which,
654 particularly in this study, ranges from -0.17±0.15 nmol kg^{-1} in February to 0.6±0.18 nmol kg^{-1} in
655 November. As in the case of N_2O, in order to evaluate the short-term variability, CH_4 anomalies,
656 calculated as the difference between cruise-averaged CH_4 concentration and each individual
657 CH_4 observation, were examined in relation to SST anomalies, but no significant correlation with
658 SST was observed.
659
660 Applying equation 2, and using the N_2O and CH_4 concentrations in water given in Table 2, air-
661 sea fluxes of N_2O and CH_4 were calculated (Table 2). Since k_w formulation is a non-linear
662 function of wind speed, the air-sea exchange was computed first from the individual data pairs
663 and subsequently averaged for each cruise. The resulting N_2O air-sea flux (F_{N2O}) value
664 oscillated between 1.17±0.09 μmol m^{-2} d^{-1} in August 2011 and 0.02±0.06 in November 2011.
665 However, the N_2O anomalies observed during each cruise (Table 2 and Fig. 2) due to vertical
666 mixing are higher than the seasonal variability of ΔN_2O and F_{N2O} (Table 2), and increase

667 markedly towards the east. The magnitude of the N_2O fluxes depends strongly on the ΔN_2O,
668 and, although higher surface N_2O concentrations were observed in winter, both the maximum
669 supersaturation and F_{N2O} occurred during the summer month. Nevertheless, it must be stated
670 that the net annual air-sea exchange of N_2O was calculated from the cruise-averaged flux data
671 grouped into seasons (Fig. 6). On an annual basis, the net N_2O flux in the Strait of Gibraltar is
672 0.35±0.27 μmol m^{-2} d^{-1} resulting in a near neutral transfer with the atmosphere. This behavior is
673 consistent with that of most of the ocean surface in the North Atlantic, which shows a negligible
674 N_2O net flux with the atmosphere (Nevison et al., 2003; Walter et al., 2006; Forster et al., 2009).
675 These low N_2O flux values contrast with the high air-water N_2O exchange values calculated in
676 the north-eastern shelf of the Gulf of Cadiz, which varied between 2.8±2.9 μmol m^{-2} d^{-1} and
677 15.3±9.3 μmol m^{-2} d^{-1} in winter and summer, respectively (Ferrón et al., 2010b). As mentioned
678 above, the intense gradient of terrestrial inputs of N_2O precursors in the continental shelf, as
679 well as the high microbial activity present normally in coastal areas in relation to the open
680 ocean, may be the main factors underlying the differences observed between the two
681 neighboring areas.
682 With regard to CH_4, the Strait of Gibraltar behaves as a sink in February (-0.15±0.12 μmol m^2d^1)
683 and as a source in May (0.70±0.08 μmol m^{-2} d^{-1}) and November (1.68±0.50 μmol m^{-2} d^{-1}) (Table
684 2). The sink/source status of the Strait is consistent with the observations by Ferrón et al.
685 (2010a) in the north-eastern shelf waters of the Gulf of Cadiz for February and May
686 respectively, although those authors report CH_4 flux values one order of magnitude higher than
687 those shown here. In that case, the levels of CH_4 saturation were directly influenced by
688 continental inputs and benthic fluxes, and changed seasonally depending on the water
689 temperature (positively correlated) and the magnitude of the freshwater discharge (Ferrón et al.,
690 2010a).
691
692 **3.5. N_2O balance in the Strait of Gibraltar**
693
694 To assess the main mechanism influencing inputs and outputs of N_2O in the Strait of Gibraltar,
695 N_2O fluxes associated with the two main water flows has been compared to the air-sea
696 exchange of N_2O at the surface of the waters in the region. The N_2O exchange between the
697 Atlantic and the Mediterranean has been computed according to equation 4, thereby requiring

698 an estimate of the average [N_2O] for the AIW and MOW layers at the Espartell Sill. As illustrated
699 in Fig. 2, [N_2O] distribution is characterized by an increasing vertical gradient everywhere in the
700 channel, reflecting the confluence of water masses with distinctive N_2O signatures. Overall, the
701 averaged [N_2O] in the AIW penetrating into the Strait is 9.00±1.18 nmol kg^{-1} (n=18 in water with
702 S< 37 at St. 1). Higher levels of [N_2O] were detected in the MOW, with a more uniform vertical
703 distribution than in the upper AIW layer and an average concentration of 10.26±0.27 nmol kg^{-1}
704 (n=17 in waters with S>37 at St. 1). When net fluxes are calculated a net export from the
705 Mediterranean to the Atlantic is obtained, which amounts to 682±20 mmol s^{-1}. Considering a
706 total surface area of the Strait of Gibraltar of 1500 km^2, the net export of N_2O per unit of area is
707 39 μmol m^{-2} d^{-1} towards the Atlantic. This flux can be now compared with the calculated annual
708 mean air-sea N_2O flux of the total N_2O emission by the Strait of Gibraltar equal to 0.35 μmol m^{-2}
709 d^{-1}. Therefore, the export of N_2O from the Mediterranean towards the North Atlantic through the
710 Strait of Gibraltar is more than one hundred times higher than the net emission of N_2O to the
711 atmosphere. Given to the complexity of the water circulation in the Strait of Gibraltar, especially
712 due to the high tidal variability that complicates the observational strategy for measuring both
713 the water transport and the biogeochemical distribution pattern, one of the most debated issues
714 for estimating the exchange of water and substances through the Strait is the section where the
715 exchange is evaluated. For this study, water exchange and N_2O concentrations were assessed
716 at Station 1, located at the Espartell Sill, where the N_2O enrichment observed in the upper layer
717 due to the tidal-induced vertical mixing, do not affect our computations. Previous studies
718 (García-Lafuente et al., 2007, Sanchez-Roman et al., 2009), have taken the Espartel sill as the
719 reference spot for monitoring water exchange through the Strait, since at this particular section,
720 tidal currents in the MOW layer are not strong enough to reverse the subinertial flow and
721 consequently the fraction of MOW that returns to the Mediterranean basin can be considered
722 negligible.
723 Although the results of this study reveal an increase of N_2O content at the surface layer in the
724 eastern entrance of the Strait, which may be associated with the tidal-induced mixing
725 processes, this short time-scale variability does not mask the seasonal variability and hence,
726 N_2O concentration at the surface remains close to the equilibrium with the atmosphere,
727 reflecting the annual seasonal cycle. It can then be concluded that advection associated with

728 the Atlantic and Mediterranean flows in the Strait of Gibraltar is the main mechanism governing
729 the N_2O distribution in the region, being two orders of magnitude larger than the air-sea
730 transport of N_2O.
731 According to the observed distribution pattern of CH_4 in the water column, which does not
732 reflect a distribution in two layers unlike that observed for N_2O, and also due to the low gradient
733 of CH_4 concentrations detected between the AIW and the MOW, more observations are needed
734 to make a reliable evaluation of the CH_4 exchanged between Atlantic and Mediterranean
735 waters.
736
737 **4. Conclusions**
738
739 The vertical distribution of N_2O concentrations in the Strait of Gibraltar presents typical features
740 linked to the bi-layer circulation scheme proposed for this region, where the strong lateral
741 advection and water mixing at the interface between the Atlantic and Mediterranean waters
742 masses with different N_2O signatures govern its spatial distribution. The SAW is characterized
743 by N_2O values in near-equilibrium with the atmosphere, with seasonal variability closely
744 associated with the annual temperature cycle. In contrast, the deeper MOW, and to a lesser
745 extent the NACW, show concentrations of N_2O markedly far from the saturation concentrations.
746 Data suggest that production by nitrification is the process underlying the N_2O supersaturation
747 observed in the NACW and the MOW. The vertical distribution of CH_4 exhibits a high temporal
748 variability in the upper Atlantic layer, with values near saturation concentrations in February and
749 oversaturation during May and November. On the other hand, the notable undersaturation of
750 CH_4 in the MOW may reflect intense CH_4 oxidation activity at deep and intermediate levels in
751 the Mediterranean basin. Annually, the Strait of Gibraltar behaves as a very limited source for
752 atmospheric N_2O, with CH_4 also being emitted in spring and fall but absorbed in winter.
753 However, the main contributor to the N_2O balance in the region is horizontal transport, as the
754 N_2O exchange between basins found is much greater than that produced by air-sea
755 transference. The N_2O and CH_4 observations provided in this study represent valuable
756 information from a region of considerable geographic and oceanographic relevance - the only
757 marine connection between the Atlantic and Mediterranean basins.
758

Acknowledgments.

The excellent co-operation of the captains and the crews of *R/V García del Cid, Cornide de Saavedra, Hesperides and Socib* are gratefully acknowledged. We also thank María Ferrer-Marco and Manuel Arjonilla for collection and measurement of the samples. The authors are also grateful to the Spanish "Puertos del Estado" for providing the meteorological data. Comments by two anonymous reviewers significantly improved this paper. Funding for this work was provided by the INGOS (Grant agreement 284274), CARBOCHANGE IP (264879GOCE) and PERSEUS of the European Commission, the CATARINA Project supported by the MICINN and co-funded by FEDER (CTM2010-17141/MAR)) and OSIMON project funded by the Regional Government of Galicia (Xunta de Galicia, 09MDS035402PR).

References

Aït-Ameur, N., Goyet, C., 2006. Distribution and transport of natural and anthropogenic CO2 in the Gulf of Cádiz. Deep Sea Res. Part II Top. Stud. Oceanogr. 53, 11–13, 1329–1343. doi: 10.1016/j.dsr2.2006.04.003

Álvarez, M., Pérez, F.F., Shoosmith, D.R., Bryden, H.L., 2005. Unaccounted role of Mediterranean Water in the drawdown of anthropogenic carbon. J. Geophys. Res. 110, C9, C09S03.

Armi, L., Farmer, D., 1985. The internal hydraulics of the Strait of Gibraltar and associated sill and narrows. Oceanologica Acta 8 (1), 37–46.

Bakker, D.C.E., Bange, H.W., Gruber, N., Johannessen, T., Upstill-Goddard, R.C., Borges, A.V., Delille, B., Löscher, C.R., Naqvi, S.W.A., Omar, A.M., Santana-Casiano, J.M., 2014. Air-Sea Interactions of Natural Long-Lived Greenhouse Gases (CO2, N2O, CH4) in a Changing Climate, in: Liss, P.S., Johnson, M.T. (Eds.), Ocean-Atmosphere Interactions of Gases and Particles, Springer Earth System Sciences. Springer Berlin Heidelberg, pp. 113–169.

Bange, H. W., Bell, T. G., Cornejo, M., Freing, A., Uher, G., Upstill-Goddard, R. C., and Zhang, G.: MEMENTO: a proposal to develop a database of marine nitrous oxide and methane measurements, Environ. Chem., 6, 195–197, doi:10.1071/en09033, 2009

Bange, H.W., Bergmann, K., Hansen, H.P., Kock, A., Koppe, R., Malien, F., Ostrau, C., 2010. Dissolved methane during hypoxic events at the Boknis Eck time series station (Eckernförde Bay, SW Baltic Sea). Biogeosciences 7, 4, 1279–1284. doi: 10.5194/bg-7-1279-2010

Bethoux, J.P., Boukhary, M.S.E., Ruiz-Pino, D., Morin, P., Copin-Montégut, C., 2005. Nutrient, Oxygen and Carbon Ratios, CO2 Sequestration and Anthropogenic Forcing in the Mediterranean Sea, in: Saliot, A. (Ed.), The Mediterranean Sea, Handbook of Environmental Chemistry. Springer Berlin Heidelberg, pp. 67–86.

799 Boetius, A., Ravenschlag, K., Schubert, C.J., Rickert, D., Widdel, F., Gieseke, A., Amann, R.,
800 Jørgensen, B.B., Witte, U., Pfannkuche, O. 2000. A marine microbial consortium
801 apparently mediating anaerobic oxidation of methane. Nature 407, 6804, 623–626. doi:
802 10.1038/35036572
803 Boyce, F.M., 1975. Internal waves in t(Carini et al., 2014)he Strait of Gibraltar. Deep Sea Res. 22,
804 597–610.
805 Bray, N.A., Ochoa, J., Kinder, T.H., 1995. The role of the interface in exchange through the Strait
806 of Gibraltar. J. Geophys. Res. Oceans 100, C6, 10755–10776. doi: 10.1029/95JC00381
807 Bruno, M., Juan Alonso, J., Cózar, A., Vidal, J., Ruiz-Cañavate, A., Echevarría, F., Ruiz, J., 2002.
808 The boiling-water phenomena at Camarinal Sill, the strait of Gibraltar. Deep Sea Res. Part
809 II Top. Stud. Oceanogr., Canary Islands, Azores, Gibraltar Observations (Canigo) Volume
810 II : Studies of the Azores and Gibraltar regions 49, 19, 4097–4113. doi: 10.1016/S0967-
811 0645(02)00144-3.
812 Carini, P., White, A.E., Campbell, E.O., Giovannoni, S.J., 2014. Methane production by phosphate-
813 starved SAR11 chemoheterotrophic marine bacteria. Nat Commun 5.
814 Ciais, P., C. Sabine, G. Bala, L. Bopp, V. Brovkin, J. Canadell, A. Chhabra, R. DeFries, J.
815 Galloway, M. Heimann, C. Jones, C. Le Quéré, R.B. Myneni, S. Piao and P. Thornton,
816 2013: Carbon and Other Biogeochemical Cycles. In: Climate Change 2013: The Physical
817 Science Basis. Contribution of Working Group I to the Fifth Assessment Report of the
818 Intergovernmental Panel on Climate Change [Stocker, T.F., D. Qin, G.-K. Plattner, M.
819 Tignor, S.K. Allen, J. Boschung, A. Nauels, Y. Xia, V. Bex and P.M. Midgley (eds.)].
820 Cambridge University Press, Cambridge, United Kingdom and New York, NY, USA.
821 Codispoti, L.A., 2010. Interesting Times for Marine N2O. Science 327, 5971, 1339–1340. doi:
822 10.1126/science.1184945
823 Codispoti, L.A., Yoshinari, T., Devol, A.H., 2005. Suboxic respiration in the oceanic water column.
824 Oxford University Press, pp. 225–247.
825 Crutzen P J. The influence of nitrogen oxides on the atmospheric ozone content. Quarterly Journal
826 Review of the Meteorological Society. 1970; 96:320-325.
827 Crutzen, P.J., 1991. Methane's sinks and sources. Nature 350 (6317), 380–381
828 Dachs, J., Bayona, J.M., Raoux, C., Albaigés, J., 1997. Spatial, Vertical Distribution and Budget of
829 Polycyclic Aromatic Hydrocarbons in the Western Mediterranean Seawater. Environ. Sci.
830 Technol. 31, 3, 682–688. doi: 10.1021/es960233j
831 Dafner, E., González-Dávila, M., Magdalena Santana-Casiano, J., Sempéré, R., 2001. Total
832 organic and inorganic carbon exchange through the Strait of Gibraltar in September 1997.
833 Deep Sea Res. Part Oceanogr. Res. Pap. 48, 5, 1217–1235. doi: 10.1016/S0967-
834 0637(00)00064-9
835 Dafner, E.V., Boscolo, R., Bryden, H.L., 2003. The N:Si:P molar ratio in the Strait of Gibraltar.
836 Geophys. Res. Lett. 30, 10, n/a–n/a. doi: 10.1029/2002GL016274

de la Paz, M., Debelius, B., Macías, D., Vázquez, A., Gómez-Parra, A., Forja, J.M., 2008. Tidal-induced inorganic carbon dynamics in the Strait of Gibraltar. Cont. Shelf Res. 28, 14, 1827–1837. doi: 10.1016/j.csr.2008.04.012

de la Paz, M., Huertas, E.M., Padín, X.-A., Gónzalez-Dávila, M., Santana-Casiano, M., Forja, J.M., Orbi, A., Pérez, F.F., Ríos, A.F., 2011. Reconstruction of the seasonal cycle of air–sea CO2 fluxes in the Strait of Gibraltar. Mar. Chem. 126, 1–4, 155–162. doi: 10.1016/j.marchem.2011.05.004

De Angelis MA, Lee C ,1994. Methane production during zooplankton grazing on marine phytoplankton. Limnol Oceanogr 39:1298–1308

Dlugokencky, E.J., Steele, L.P., Lang, P.M. and Masarie, K.A. 1994. The growth rate and distribution of atmospheric methane. *Journal of Geophysical Research* **99**: 17,021-17,043.

Dore, J.E., Popp, B.N., Karl, D.M., Sansone, F.J., 1998. A large source of atmospheric nitrous oxide from subtropical North Pacific surface waters. Nature 396, 6706, 63–66. doi: 10.1038/23921

Echevarría, F., García Lafuente, J., Bruno, M., Gorsky, G., Goutx, M., González, N., García, C.M., Gómez, F., Vargas, J.M., Picheral, M., Striby, L., Varela, M., Alonso, J.J., Reul, A., Cózar, A., Prieto, L., Sarhan, T., Plaza, F., Jiménez-Gómez, F., 2002. Physical–biological coupling in the Strait of Gibraltar. Deep Sea Res. Part II Top. Stud. Oceanogr. 49, 19, 4115–4130. doi: 10.1016/S0967-0645(02)00145-5.

Elbaz-Poulichet, F., C. Guieu, and N. H. Morley (2001), A reassessment of trace metal budgets in the western Mediterranean Sea, Mar. Pollut. Bull., 42(8), 623–627, doi:10.1016/S0025-326X(01)00065-0.

Ferrón, S., Ortega, T., Forja, J.M., 2010a. Temporal and spatial variability of methane in the north-eastern shelf of the Gulf of Cádiz (SW Iberian Peninsula). J. Sea Res. 64, 3, 213–223. doi: 10.1016/j.seares.2010.02.007

Ferrón, S., Ortega, T., Forja, J.M., 2010b. Nitrous oxide distribution in the north-eastern shelf of the Gulf of Cádiz (SW Iberian Peninsula). Mar. Chem. 119, 1–4, 22–32. doi: 10.1016/j.marchem.2009.12.003

Flecha, S., Pérez, F.F., Navarro, G., Ruiz, J., Olivé, I., Rodríguez-Gálvez, S., Costas, E., Huertas, I.E., 2012. Anthropogenic carbon inventory in the Gulf of Cádiz. J. Mar. Syst. 92, 1, 67–75. doi: 10.1016/j.jmarsys.2011.10.010

Forster, G., Upstill-Goddard, R.C., Gist, N., Robinson, C., Uher, G., Woodward, E.M.S., 2009. Nitrous oxide and methane in the Atlantic Ocean between 50°N and 52°S: Latitudinal distribution and sea-to-air flux. Deep Sea Res. Part II Top. Stud. Oceanogr. 56, 15, 964–976. doi: 10.1016/j.dsr2.2008.12.002

Freing, A., Wallace, D.W.R., Tanhua, T., Walter, S., Bange, H.W., 2009. North Atlantic production of nitrous oxide in the context of changing atmospheric levels. Glob. Biogeochem. Cycles 23, 4, n/a–n/a. doi: 10.1029/2009GB003472.

Freing A, Wallace DWR, Bange HW (2012) Global oceanic production of nitrous oxide (N2O). Philos Trans R Soc B 367:1245–1255

García Lafuente, J., Álvarez Fanjul, E., Vargas, J.M., Ratsimandresy, A.W., 2002. Subinertial variability in the flow through the Strait of Gibraltar. J. Geophys. Res. Oceans 107, C10, 32–1–31–9. doi: 10.1029/2001JC001104

García Lafuente, J., Sánchez Román, A., Díaz del Río, G., Sannino, G., Sánchez Garrido, J.C., 2007. Recent observations of seasonal variability of the Mediterranean outflow in the Strait of Gibraltar. J. Geophys. Res. Oceans 112, C10, n/a–n/a. doi: 10.1029/2006JC003992

Garçon, V.C., Bell, T.G., Wallace, D., Arnold, S.R., Baker, A., Bakker, D.C.E., Bange, H.W., Bates, N.R., Bopp, L., Boutin, J., Boyd, P.W., Bracher, A., Burrows, J.P., Carpenter, L.J., Leeuw, G. de, Fennel, K., Font, J., Friedrich, T., Garbe, C.S., Gruber, N., Jaeglé, L., Lana, A., Lee, J.D., Liss, P.S., Miller, L.A., Olgun, N., Olsen, A., Pfeil, B., Quack, B., Read, K.A., Reul, N., Rödenbeck, C., Rohekar, S.S., Saiz-Lopez, A., Saltzman, E.S., Schneising, O., Schuster, U., Seferian, R., Steinhoff, T., Traon, P.-Y.L., Ziska, F., 2014. Perspectives and Integration in SOLAS Science, in: Liss, P.S., Johnson, M.T. (Eds.), Ocean-Atmosphere Interactions of Gases and Particles, Springer Earth System Sciences. Springer Berlin Heidelberg, pp. 247–306.

Gascard, J.-C., Richez, Z., 1985. Water masses and circulation in the western Alboran Sea, and in the Straits of Gibraltar. Prog. Oceanogr. 15, 216.

Goreau, T.J., Kaplan, W.A., Wofsy, S.C., McElroy, M.B., Valois, F.W., Watson, S.W., 1980. Production of NO2- and N2O by Nitrifying Bacteria at Reduced Concentrations of Oxygen. Appl. Environ. Microbiol. 40, 3, 526–532.

Grasshoff, K., Ehrhardt, M., Kremling, K., 1983. Methods of Seawater Analysis, 2nd ed. Verlag Chemie, Weinheim, Germany.

Huertas, I.E., Ríos, A.F., García-Lafuente, J., Makaoui, A., Rodríguez-Gálvez, S., Sánchez-Román, A., Orbi, A., Ruíz, J., Pérez, F.F., 2009. Anthropogenic and natural CO2 exchange through the Strait of Gibraltar. Biogeosciences 6, 647–662.

Huertas, I.E., Ríos, A.F., García-Lafuente, J., Navarro, G., Makaoui, A., Sánchez-Román, A., Rodriguez-Galvez, S., Orbi, A., Ruíz, J., Pérez, F.F., 2012. Atlantic forcing of the Mediterranean oligotrophy. Glob. Biogeochem. Cycles 26, 2, n/a–n/a. doi: 10.1029/2011GB004167

Karl, D., & Tilbrook, B. (1994). Production and transport of methane in oceanic particulate organic matter Nature, 368 (6473), 732-734 DOI: 10.1038/368732a0

Karl DM, Beversdorf L, Björkman KM, Church MJ, Martinez A, Delong EF (2008) Aerobic production of methane in the sea. Nat Geosci 1:473–478.

Keir, R.S., Greinert, J., Rhein, M., Petrick, G., Sültenfuß, J., Fürhaupter, K., 2005. Methane and methane carbon isotope ratios in the Northeast Atlantic including the Mid-Atlantic Ridge (50°N). Deep Sea Res. Part Oceanogr. Res. Pap. 52, 6, 1043–1070. doi: 10.1016/j.dsr.2004.12.006

Large, W.G., Pond, S., 1981. Open ocean-momentum flux measurements in moderate to strong winds. J. Phys. Oceanogr. 11, 324–336.

916 Macías, D., Lubián, L.M., Echevarría, F., Huertas, I.E., García, C.M., 2008. Chlorophyll maxima
917 and water mass interfaces: Tidally induced dynamics in the Strait of Gibraltar. Deep Sea
918 Res. Part Oceanogr. Res. Pap. 55, 7, 832–846. doi: 10.1016/j.dsr.2008.03.008
919 Macías, D., Martin, A.P., García-Lafuente, J., García, C.M., Yool, A., Bruno, M., Vázquez-Escobar,
920 A., Izquierdo, A., Sein, D.V., Echevarría, F., 2007a. Analysis of mixing and biogeochemical
921 effects induced by tides on the Atlantic–Mediterranean flow in the Strait of Gibraltar through
922 a physical–biological coupled model. Prog. Oceanogr. 74, 2–3, 252–272. doi:
923 10.1016/j.pocean.2007.04.006
924 Macías, D., Navarro, G., Echevarría, F., García, C.M., Cueto, J.L., 2007b. Phytoplankton pigment
925 distribution in the northwestern Alboran Sea and meteorological forcing: A remote sensing
926 study. J. Mar. Res. 65, 4, 523–543. doi: 10.1357/002224007782689085
927 Minas, H.J., Coste, B., Le Corre, P., Minas, M., Raimbault, P., 1991. Biological and geochemical
928 signatures associated with the water circulation through the Strait of Gibraltar and in the
929 western Alboran Sea. J. Geophys. Res. Oceans 96, C5, 8755–8771. doi:
930 10.1029/91JC00360
931 Naqvi, S.W.A., Bange, H.W., Farías, L., Monteiro, P.M.S., Scranton, M.I., Zhang, J., 2010. Marine
932 hypoxia/anoxia as a source of CH4 and N2O. Biogeosciences 7, 7, 2159–2190. doi:
933 10.5194/bg-7-2159-2010
934 Naranjo, C., Garcia-Lafuente, J., Sannino, G., Sanchez-Garrido, J., 2014. How much do tides
935 affect the circulation of the Mediterranean Sea? From local processes in the Strait of
936 Gibraltar to basin-scale effects. Prog. Oceanogr. doi: 10.1016/j.pocean.2014.06.005
937 Navarro, G., Ruiz, J., 2006. Spatial and temporal variability of phytoplankton in the Gulf of Cádiz
938 through remote sensing images. Deep-Sea Research Part II: Topical Studies in
939 Oceanography 53, 11-13, 1241–1260. doi: 10.1016/j.dsr2.2006.04.014
940 Neill, C., Johnson, K.M., Lewis, E., Wallace, D.W., 1997. Accurate headspace analysis of fCO_2 in
941 discrete water samples using batch equilibration. Limnol. Oceanogr. 42, 1774–1783.
942 Nevison, C. D., Weiss, R. F. and Erickson, D. J. 1995. Global oceanic emissions of nitrous oxide.
943 *J. Geophys. Res. Oceans* **100**(C8), 15 809– 820.
944 Nevison, C., Butler, J.H., Elkins, J.W., 2003. Global distribution of N2O and the ΔN2O-AOU yield in
945 the subsurface ocean. Glob. Biogeochem. Cycles 17 (4) 1119,doi:10.1029/2003GB002068
946 Niemann, H., Duarte, J., Hensen, C., Omoregie, E.,Magalhães, V.H., Elvert, M., Pinheiro, L.M.,
947 Kopf, A., Boetius, A., 2006. Microbial methane turnover at mud volcanoes of the Gulf of
948 Cadiz. Geochim. Cosmochim. Acta 70, 5336–5355
949 Nightingale, P.D., Liss, P.S., Schlosser, P., 2000. Measurements of air-sea gas transfer during an
950 open ocean algal bloom. Geophys. Res. Lett. 27, 14, 2117–2120. doi:
951 10.1029/2000GL011541
952 Oudot, C., Jean-Baptiste, P., Fourré, E., Mormiche, C., Guevel, M., Ternon, J.F., Le Corre, P.,
953 2002. Transatlantic equatorial distribution of nitrous oxide and methane. Deep Sea Res.
954 Part Oceanogr. Res. Pap. 49, 7, 1175–1193.

955 Peliz, A., Marchesiello, P., Santos, A.M.P., Dubert, J., Teles-Machado, A., Marta-Almeida, M., Le
956 Cann, B., 2009. Surface circulation in the Gulf of Cadiz: 2. Inflow-outflow coupling and the
957 Gulf of Cadiz slope current. J. Geophys. Res. Oceans 114, C3, n/a–n/a. doi:
958 10.1029/2008JC004771
959 Pérez, F., Mintrop, L., Llinás, O., González-Dávila, M., Castro, C.G., Álvarez, M., Körtzinger, A.,
960 Santana-Casiano, M., Rueda, M.J., Ríos, A.F., 2001. Mixing analysis of nutrients, oxygen
961 and inorganic carbon in the Canary Islands region. J. Mar. Syst. 28, 183–201. doi:
962 10.1016/S0924-7963(01)00003-3
963 Periañez, R., 2008. A Modelling Study on 137cs and 239,240pu Behaviour in the Albora?N Sea,
964 Western Mediterranean. *En: Journal of environmental radioactivity*. 2008. Vol. 99. Núm. 4.
965 Pag. 694-715
966 Pollard, R.T., Griffttths, M.J., Cunningham, S.A., Read, J.F., Pérez, F.F., Ríos, A.F., 1996. Vivaldi
967 1991 - A study of the formation, circulation and ventilation of Eastern North Atlantic Central
968 Water. Prog. Oceanogr. 37, 167–192. doi: 10.1016/S0079-6611(96)00008-0
969 Pujo-Pay, M., Conan, P., Oriol, L., Cornet-Barthaux, V., Falco, C., Ghiglione, J.-F., Goyet, C.,
970 Moutin, T., Prieur, L., 2011. Integrated survey of elemental stoichiometry (C, N, P) from the
971 western to eastern Mediterranean Sea. Biogeosciences 8, 4, 883–899. doi: 10.5194/bg-8-
972 883-2011
973 Reeburgh WS (2007) Oceanic methane biogeochemistry. Chem. Rev 107(2):486–513
974 Rhee TS, Kettle AJ, Andreae MO (2009) Methane and nitrous oxide emissions from the ocean: a
975 reassessment using basin-wide observations in the Atlantic. J Geophys Res 114,D12304.
976 doi:10.1029/2008JD011662
977 Ríos, A.F., Perez, F.F., Fraga, F., 1992. Water masses in the upper and middle North Atlantic
978 Ocean east of the Azores. Deep Sea Res. Part Oceanogr. Res. Pap. 39, 645–658. doi:
979 10.1016/0198-0149(92)90093-9
980 Roether, W., Schlitzer, R., 1991. Eastern Mediterranean deep water renewal on the basis of
981 chlorofluoromethane and tritium data. Dyn. Atmospheres Oceans, The Mediterranean Sea
982 15, 3–5, 333–354. doi: 10.1016/0377-0265(91)90025-B
983 Sánchez-Román,A., G.Sannino, J.Garcıa-Lafuente, A. Carillo, and F. Criado-Aldeanueva 2009,
984 Transport estimates at the western section of the Strait of Gibraltar: A combined
985 experimental and numerical modelling study,J. Geophys. Res., 114, C06002, doi:
986 10.1029/2008JC005023
987 Schmidt S., 2006. Impact of the Mediterranean Outflow Water on particle dynamics in intermediate
988 waters of the North-East Atlantic, as revealed by 234 Th and 228 Th. Marine Chemistry
989 100:289–298
990 Schroeder, K., García-Lafuente, J., Josey, S.A., Artale, V., Buongiorno Nardelli, B., Carrillo, A.,
991 Gacic, M., Gasparini, G.P., Herrmann, M., Lionello, P., Ludwig, W., Millot, C., Özsoy, E.,
992 Pisacane, G., Sánchez-Garrido, J.C., Sannino, G., Santoleri, R., Somot, S., Struglia, M.,
993 Stanev, E., Taupier-Letage, I., Tsimplis, M.N., Vargas-Yáñez, M., Zervakis, V., Zodiatis, G., 2012.
994 Circulation of the Mediterranean Sea and its variability, in: The Climate of the

995 Mediterranean Region: From the Past to the Future [Eds. P. Lionello]. Elsevier, London,
996 pp. 187–238.
997 Scranton, M. I. and P. G. Brewer 1977. Occurrence of methane in the near-surface waters of the
998 western subtropical North Atlantic. Deep-Sea Research, v. 24, 127-138.
999 Shakhova, N., Semiletov, I., Leifer, I., Sergienko, V., Salyuk, A., Kosmach, D.,
1000 Chernykh, D., Stubbs, C., Nicolsky, D., Tumskoy, V., Gustafsson, Ö., 2014. Ebullition and storm-
1001 induced methane release from the East Siberian Arctic Shelf. Nat. Geosci. 7, 1, 64–70. doi:
1002 10.1038/ngeo2007
1003 Somoza, L., Diaz-Del-Rio, V., Vaszquez, J.T., Pinheiro, L.M., Hernandez-Molina, F.J., 2002.
1004 Numerous methane gas-related sea floor structures identified in Gulf of Cadiz. EOS 83,
1005 541–547.
1006 Soto-Navarro, J., F. Criado-Aldeanueva, J. García-Lafuente, and A. Sánchez-Román (2010),
1007 Estimation of the Atlantic inflow through the Strait of Gibraltar from climatological and in
1008 situ data, J. Geophys. Res., 115, C10023, doi:10.1029/2010JC006302
1009 Stöven, T., Tanhua, T., 2014. Ventilation of the Mediterranean Sea constrained by multiple
1010 transient tracer measurements. Ocean Sci 10, 3, 439–457. doi: 10.5194/os-10-439-2014
1011 Tanhua, T., Hainbucher, D., Schröder, K., Cardin, V., Álvarez, M., Civitarese, G., 2013. The
1012 Mediterranean Sea system: a review and an introduction to the special issue. Ocean Sci
1013 Discuss 10, 2, 581–617. doi: 10.5194/osd-10-581-2013
1014 Upstill-Goddard, R.C., Rees, A.P., Owens, N.J.P., 1996. Simultaneous high-precision
1015 measurements of methane and nitrous oxide in water and seawater by single phase
1016 equilibration gas chromatography. Deep Sea Res. Part Oceanogr. Res. Pap. 43, 10, 1669–
1017 1682. doi: 10.1016/S0967-0637(96)00074-X
1018 Unesco, 1986. Progress on oceanographic tables and standards 1983-1986. Work and
1019 recomendations of UNESCO/SCOR/ICES/IAPSO Joint panel. UNESCO Technical Papers
1020 in Marine Science 50.
1021 Van Geen, A. and E.A. Boyle (1990) Variability of trace metal fluxes through the Straits of Gibraltar,
1022 Paleoclimatol. Paleogeog. Paleoecol. 89: 65-80.
1023 Walter, S., Bange, H.W., Breitenbach, U., Wallace, D.W.R., 2006. Nitrous oxide in the North
1024 Atlantic Ocean. Biogeosciences 3, 4, 607–619.
1025 Wanninkhof, R., 1992. Relationship between wind speed and gas exchange. J Geophys Res 97,
1026 25, 7373–7382.
1027 Weiss, R.F., Price, B.A., 1980. Nitrous oxide solubility in water and seawater. Mar. Chem. 8, 4,
1028 347–359. doi: 10.1016/0304-4203(80)90024-9
1029 Wiesenburg, D.A., Guinasso Jr, N.L., 1979. Equilibrium solubilities of methane, carbon monoxide,
1030 and hydrogen in water and sea water. J. Chem. Eng. Data 24, 4, 356–360.
1031 Yoshida O, Inoue HY, Watanabe S, Suzuki K, Noriki S (2011) Dissolved methane distribution in the
1032 South Pacific and the Southern Ocean in austral summer. J Geophys Res 116,C07008.
1033 doi:10.1029/2009JC006089

Yoshinari, T., 1976. Nitrous oxide in the sea. Mar. Chem. 4, 2, 189–202. doi: 10.1016/0304-4203(76)90007-4

LIST OF FIGURES

Figure 1. Map of the study area including the bathymetry and locations of the GIFT stations.

Figure 2. Vertical distribution of potential temperature, salinity, dissolved oxygen, nitrate, nitrous oxide (N_2O) and methane (CH_4) along the Strait of Gibraltar with data corresponding to the cruise carried out in May 2013. The contour black line shows the salinity 37 isocline, to track the depth of the AMI.

Figure 3. Vertical distribution of potential temperature (θ), salinity, N_2O and CH_4 concentrations for Stations1, 2 and 3 for all the cruises carried out for the GITF series from 2001 to 2014. The red filled symbols correspond to the cruise in May 2013.

Figure 4. Scatter diagram plot of: a) potential temperature versus salinity (θ); b) AOU versus salinity; c) N_2O concentrations (filled symbols) and saturation N_2O concentrations versus salinity (open symbols); and c) CH_4 concentrations (filled symbols) and saturation CH_4 concentrations versus salinity (open symbols). Acronyms corresponding to the water masses present in the Strait (NACW, SAW and MOW) have also been included. The thermohaline properties of the AMI have been included in plot a).

Figure 5. a) N_2O excess (ΔN_2O) in relation to AOU; and (b) nitrate NO_3^{-1} for the complete GIFT database. Open symbols correspond to AIW and filled symbols to MOW; c) Ratio of ΔN_2O/AOU versus AOU for observations at depths more than 25 m. The equations for the linear regressions are: in a) $\Delta N_2O=0.28+0.018$ AOU, $r^2=0.73$; and in b) $\Delta N_2O=0.18+0.14$ NO_3-; $r^2=0.62$.

Figure 6. Annual cycle at the surface layer in the Strait of Gibraltar for: a) surface seawater temperature (SST), N_2O, N_2O saturation and N_2O air-sea fluxes; and (b) SST, CH_4, CH_4

saturation and CH_4 air-sea fluxes. For N_2O and CH_4 concentrations in surface waters, averaged data for each cruise in the upper 12 m were considered. The surface SST corresponds to the continuous temperature record for our study period (2011-2014) obtained from a buoy moored in the Gulf of Cadiz, which is part of the marine observational network of Puertos del Estado. This figure shows the climatological mean of SST calculated for that period.

Figure 7. Anomalies of N_2O versus anomalies of the sea surface temperature (SST). Anomalies were calculated as the difference between each N_2O and SST measurement at the surface and the average obtained for each cruise for surface values. The correlation line for all the data in plot is: N_2O anomaly = -3.95-0.34·SST; r^2=0.81

TABLES

Table 1. Acronyms, dates and vessels used for the campaigns referred to in this study

Campaign	Date	Ship
GIFT 0611	26 July 2011	RV *García del Cid*
GIFT 0811	4-5 August 2011	RV *Cornide de Saavedra*
GIFT 1111	10 November 2011	RV *García del Cid*
GIFT 0212	27-28 February 2012	RV *García del Cid*
GIFT 0513-Ficaram XV	23 May 2013	RV *Hespérides*
GIFT 1114	3 November 2014	RV SOCIB

Table 2. Cruise-averaged surface values (upper 12 m) for temperature, N_2O and CH_4 concentrations in water, and their respective saturation values (%), molar fraction in atmosphere, wind speed and air sea fluxes of N_2O and CH_4. The values for the atmospheric mixing ratio (xN_2O and xCH_4) are calculated using monthly mean measurements from the two meteorological stations nearest in latitude to the Strait of Gibraltar, namely Mace Head (Ireland, 53.33 ºN) and Izaña (Tenerife, Spain, 28.3 ºN) (http://ds.data.jma.go.jp/gmd/wdcgg/). The atmospheric ratios from these two meteorological stations were linearly interpolated versus latitude. The atmospheric ratios from both meteorological stations were linearly interpolated versus latitude.

Month	Temperature	N_2O (nmol kg^{-1})	CH_4(nmol kg^{-1})	X atm N_2O (ppb)	X atm CH_4 (ppb)	Sat N_2O (%)	Sat CH_4 (%)	Wind speed (m s^{-1})	Air-sea Flux N_2O (µmol m^{-2} d^{-1})	Air-sea Flux CH_4 µmol m^{-2} d^{-1})
Jul 2011	22.04	7.19±1.06	--	324	1827	104	--	2.2	0.12± 0.27	--
Aug 2011	20.20	7.91±0.66	--	324	1828	108	--	5.4	1.17± 0.09	--
Nov 2011	18.96	7.59±0.30	--	325	1855	100	--	4.9	0.02± 0.06	--
Feb 2012	15.02	8.74±0.13	2.16± 0.14	325	1859	101	93	3.7	0.11± 0.09	-0.15± 0.12
May 2013	17.75	8.00±0.30	2.66±0.17	326	1864	101	117	5.4	0.13± 0.40	0.70± 0.08
Nov 2014	17.76	8.25±0.37	2.79±0.22	326	1872	104	126	7	0.99± 0.55	1.68± 0.50

FIGURES

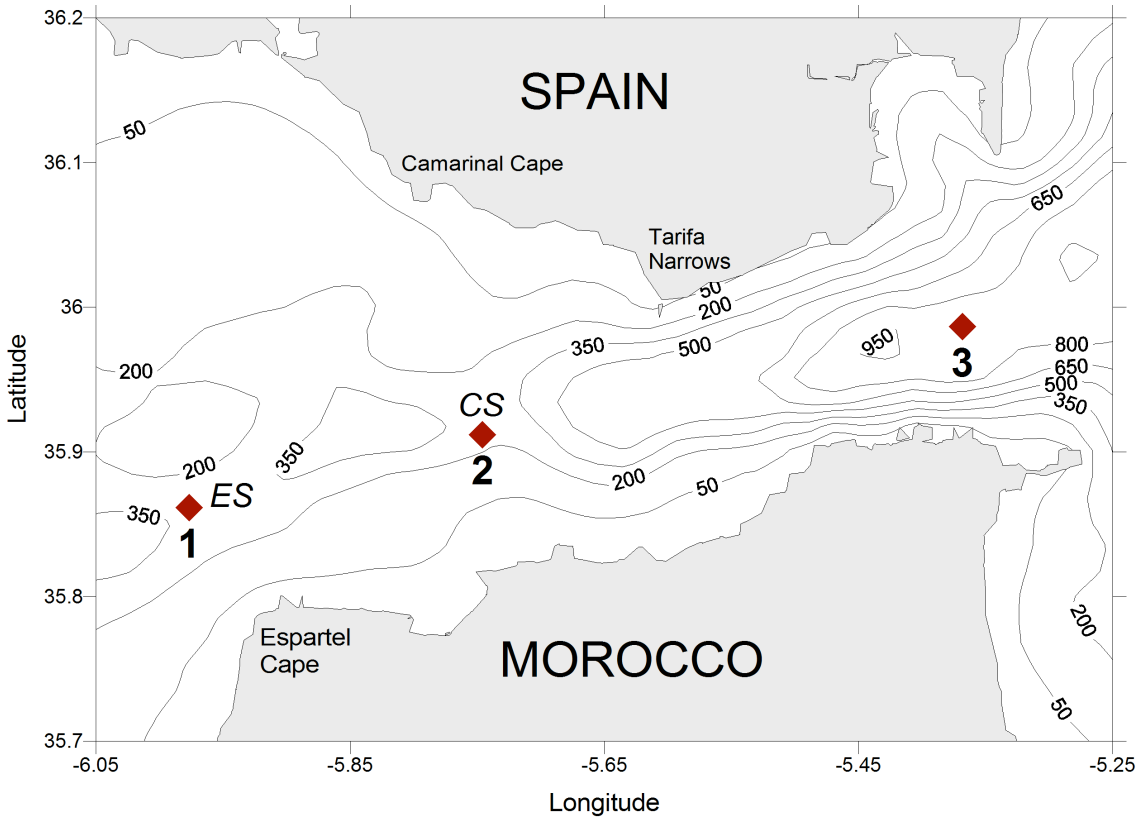
SPAIN
MOROCCO
Camarinal Cape
Tarifa
Narrows
Espartel
Cape
ES
1
CS
2
3
Latitude
Longitude
36.2
36.1
36
35.9
35.8
35.7
-6.05
-5.85
-5.65
-5.45
-5.25
50
200
350
500
650
800
950

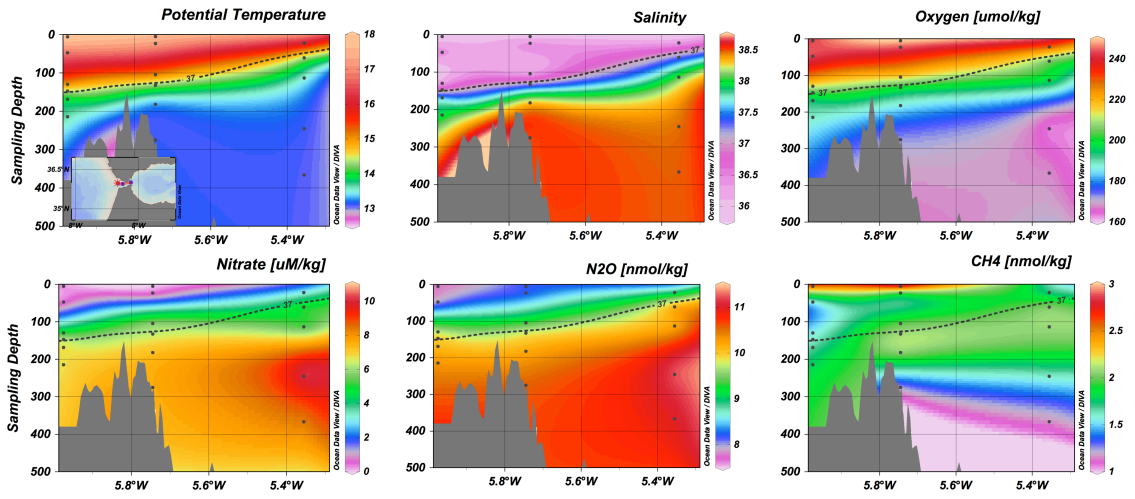
Potential Temperature
Salinity
Oxygen [umol/kg]
Nitrate [uM/kg]
N2O [nmol/kg]
CH4 [nmol/kg]
Sampling Depth
5.8°W
5.6°W
5.4°W

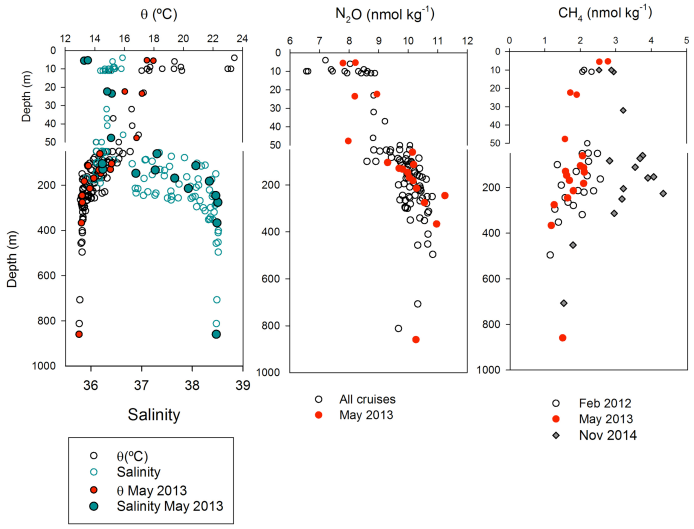
θ (ºC)
N2O (nmol kg-1)
CH4 (nmol kg-1)
Depth (m)
Salinity
θ(ºC)
Salinity
θ May 2013
Salinity May 2013
All cruises
May 2013
Feb 2012
May 2013
Nov 2014

1125
1126

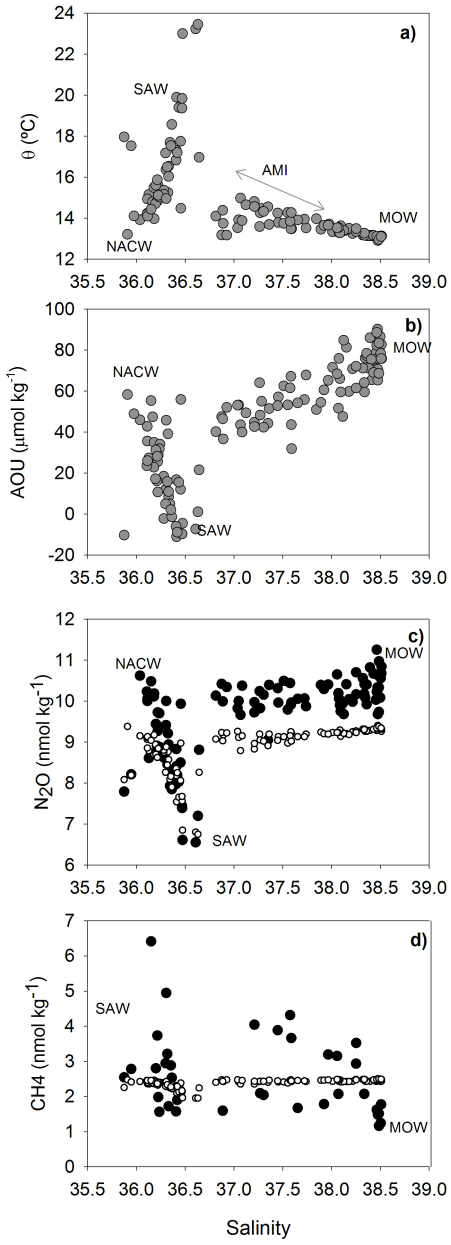

1127
1128
1129

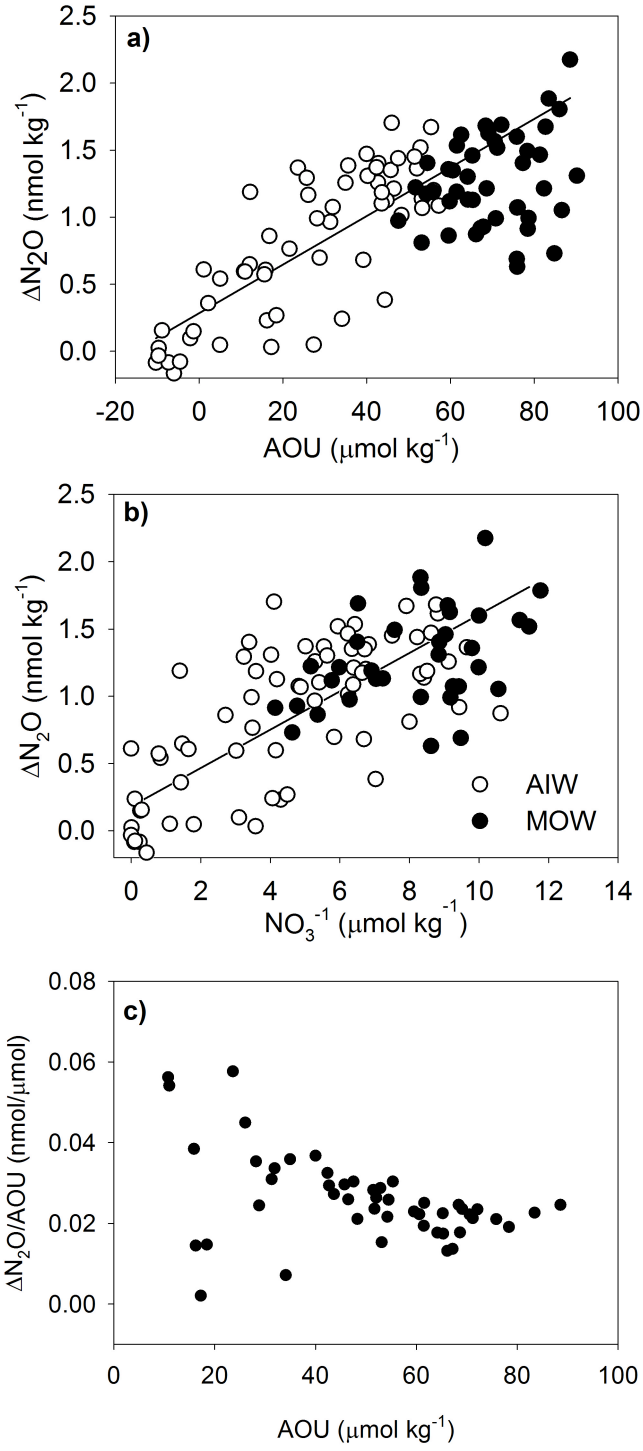
a)
b)
c)
AIW
MOW
ΔN2O (nmol kg-1)
AOU (μmol kg-1)
NO3-1 (μmol kg-1)
ΔN2O/AOU (nmol/μmol)

1130
1131

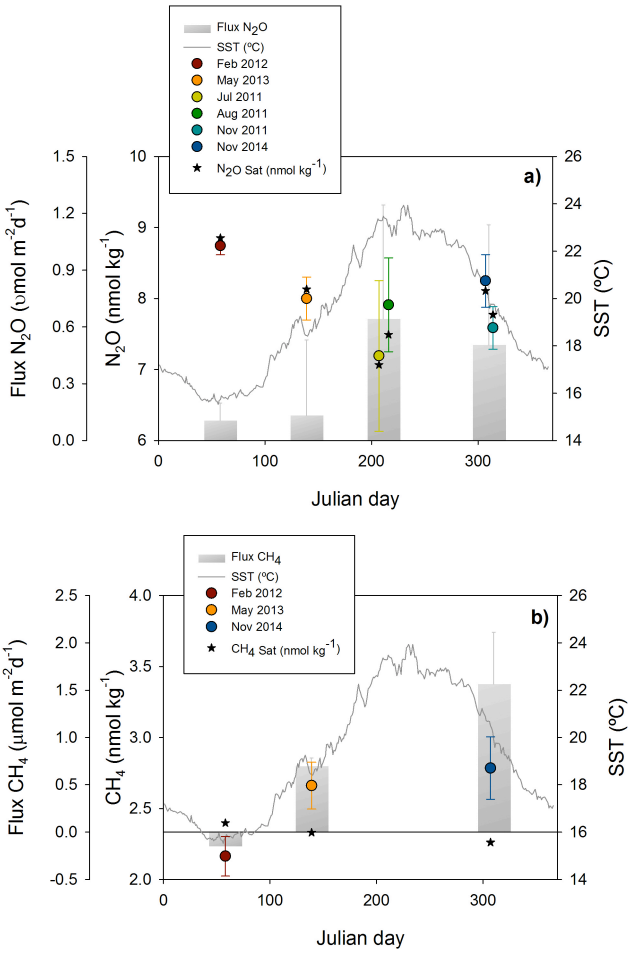

1132
1133

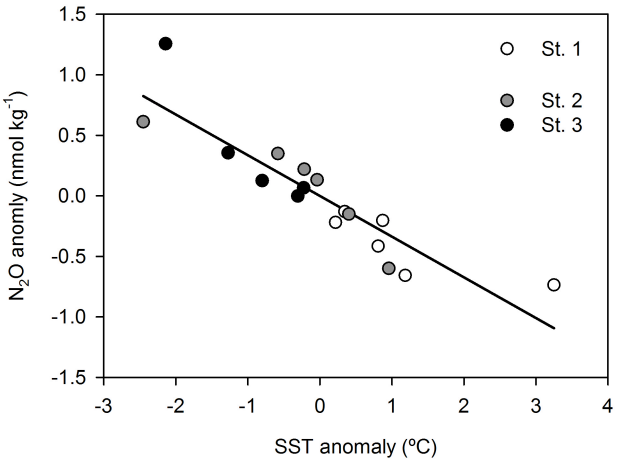

1134